© 2019. Published by The Company of Biologists Ltd | Journal of Cell Science (2019) 132, jcs226860. doi:10.1242/jcs.226860

RESEARCH ARTICLE

DSS-induced damage to basement membranes is repaired by matrix replacement and crosslinking

Angela M. Howard[1,2,3], Kimberly S. LaFever[1], Aidan M. Fenix[1], Cherie' R. Scurrah[1,3,4], Ken S. Lau[1,3,4], Dylan T. Burnette[1,3], Gautam Bhave[1,2,5], Nicholas Ferrell[5,6] and Andrea Page-McCaw[1,2,3,7,*]

ABSTRACT

Basement membranes are an ancient form of animal extracellular matrix. As important structural and functional components of tissues, basement membranes are subject to environmental damage and must be repaired while maintaining functions. Little is known about how basement membranes get repaired. This paucity stems from a lack of suitable *in vivo* models for analyzing such repair. Here, we show that dextran sodium sulfate (DSS) directly damages the gut basement membrane when fed to adult *Drosophila*. DSS becomes incorporated into the basement membrane, promoting its expansion while decreasing its stiffness, which causes morphological changes to the underlying muscles. Remarkably, two days after withdrawal of DSS, the basement membrane is repaired by all measures of analysis. We used this new damage model to determine that repair requires collagen crosslinking and replacement of damaged components. Genetic and biochemical evidence indicates that crosslinking is required to stabilize the newly incorporated repaired Collagen IV rather than to stabilize the damaged Collagen IV. These results suggest that basement membranes are surprisingly dynamic.

KEY WORDS: Basement membrane, Dextran sodium sulfate, *Drosophila*, Matrix stiffness, Midgut, Enterocytes, Collagen IV

INTRODUCTION

Basement membranes are omnipresent extracellular structures in multicellular animals. They are strong, thin sheets of extracellular matrix underlying epithelia, enveloping muscles and organs, and separating tissue layers. Basement membranes function as mechanical scaffolds to distribute cellular and tissue-level forces, and when they cannot distribute these forces, diseases such as muscular dystrophy and skin blistering result (Nyström et al., 2017). In addition to mechanical roles, basement membranes signal to cells and can tether other signaling molecules, directly and indirectly modulating cell differentiation, survival, migration and polarity of epithelial cells (Kleinman and Martin, 2005; Li et al., 2017; Wang et al., 2008; Bunt et al., 2010). Evolutionarily ancient structures, basement membranes are conserved from hydra to humans (Fidler et al., 2017). They are composed of four main components: laminin, collagen IV, perlecan, and nidogen. Super-resolution imaging of a glomerular basement membrane *in vivo* indicates that it has a laminar structure with components spatially segregated into layers (Suleiman et al., 2013), a finding consistent with *in vitro* observations that laminin and collagen IV can polymerize independently to form sheet-like polymers (Yurchenco and Furthmayr, 1984; Yurchenco et al., 1985, 1992).

The mechanical strength of basement membranes comes mainly from collagen IV, which assembles non-covalently after undergoing a conformational change mediated by high concentrations of extracellular chloride (Cummings et al., 2016). After extracellular assembly, the collagen IV network is reinforced by covalent crosslinking, the extent of which determines the stiffness of the basement membrane (Bhave et al., 2017). Crosslinking can occur at three distinct sites on a triple-helical collagen IV molecule: at the N-terminal 7S domain (Risteli et al., 1980; Langeveld et al., 1991), at lateral sites along the triple-helical domain (Yurchenco and Furthmayr, 1984), and at the C-terminal NC1 domain (Vanacore et al., 2009). The best understood of these crosslinks is between NC1 domains, which are variably crosslinked head-to-head by sulfilimine bonds, covalent linkages catalyzed by the enzyme peroxidasin using bromide as a cofactor (Bhave et al., 2012; McCall et al., 2014). There are two possible sulfilimine crosslink sites within each NC1–NC1 dimer, and up to six per NC1 hexamer that joins two triple-helical structures. However, only approximately two to four of these six sites are occupied per hexamer on average (Bhave et al., 2012; McCall et al., 2014), and the sulfilimine occupancy ratio appears to be a tissue-specific property. Like basement membranes themselves, sulfilimine crosslinks and the peroxidasin enzyme are both conserved throughout the animal kingdom (Fidler et al., 2014).

Despite their fundamental importance, questions remain about how basement membranes are assembled, and even less is known about how they are repaired after damage. As with all biological systems, basement membranes routinely get damaged. Traumatic damage like skin wounds are one obvious context for basement membrane repair. Damage and repair are also endemic processes; for example, leukocytes migrate through basement membranes and the resulting lesions are repaired to maintain mechanical integrity (Huber and Weiss, 1989). Damaged basement membrane may also play a causative role in the progression of diseases such as asthma, kidney failure and diabetes, in which altered basement membrane structures may be caused by faulty repair programs (Flood-Page et al., 2003; Sugimoto et al., 2006; Tsilibary, 2003). Further, there are diseases of the basement membrane itself (e.g. Alport syndrome, Goodpasture's syndrome, thin basement membrane disease), and understanding repair is central to treating these conditions.

There is a paucity of information on basement membrane repair, stemming from a lack of models of basement membrane damage. Questions about *de novo* basement membrane assembly have been

[1]Department of Cell and Developmental Biology, Vanderbilt University School of Medicine, Nashville, TN 37240-7935, USA. [2]Center for Matrix Biology, Vanderbilt University Medical Center, Nashville, TN 37232, USA. [3]Program in Developmental Biology, Vanderbilt University, Nashville, TN 37232, USA. [4]Epithelial Biology Center, Vanderbilt University Medical Center, Nashville, TN 37232, USA. [5]Division of Nephrology, Department of Medicine, Vanderbilt University Medical Center, Nashville, TN 37232, USA. [6]Department of Biomedical Engineering, Vanderbilt University, Nashville, TN 37235-1631, USA. [7]Program in Cancer Biology, Vanderbilt University School of Medicine, Nashville, TN 37232, USA.

*Author for correspondence (andrea.page-mccaw@vanderbilt.edu)

A.P.-M., 0000-0003-3193-5362

Received 22 October 2018; Accepted 22 February 2019

Journal of Cell Science (2019) 132, jcs226860. doi:10.1242/jcs.226860

addressed *in vitro*, in cell culture and in embryos. For example, the self-assembling nature of basement membrane components was originally discovered *in vitro* with proteins purified from EHS sarcomas (the origin of matrigel) (Yurchenco and Furthmayr, 1984; Kleinman et al., 1986, 1982). Despite their power, these systems may not be suitable for analyzing repair because *in vitro* analysis removes cells from the architectural and mechanical environment of the tissue, both of which are likely important for matrix repair. More recently, biochemical studies on matrix assembly (Fox et al., 1991; Ries et al., 2001; Takagi et al., 2003; Hopf et al., 1999) have been complemented by genetic analysis of animals with mutant basement membrane proteins, and these analyses were critical in identifying an order of assembly: laminin first, as collagen IV and nidogen each require laminin, and perlecan requires collagen IV (Pöschl et al., 2004; Urbano et al., 2009; Pastor-Pareja and Xu, 2011; Ramos-Lewis et al., 2018; Wolfstetter et al., 2019). Whole-animal mutants for basement membrane proteins are embryonic lethal, however, and the analysis of repair requires conditional mutants that can be induced temporally, after assembly has been completed. We recently published a study analyzing repair of basement membrane after an epidermal pinch wound in which the basement membrane was torn, generating a region devoid of basement membrane ∼100 µm in diameter, and found that it repaired with a scar, incorporating the known basement membrane proteins slightly differently from the order of incorporation for assembly (Ramos-Lewis et al., 2018). This assay mimics trauma wounds, with new matrix filling the breach as the cell layer migrates in; however, it is not suitable for biochemical analysis or genetic screening because the wounds are painstaking to administer and are variable and small in size. Thus, we sought a complementary assay for analyzing basement membrane repair.

Previously, we reported that when either Peroxidasin or its cofactor bromide is limiting during *Drosophila* development, basement membranes become measurably expanded and the muscles they support become deformed (McCall et al., 2014). This phenotype was first evident around the larval midgut, suggesting that this tissue has a heightened requirement for sulfilimine crosslinking. This loss-of-crosslinking phenotype appeared surprisingly similar to published images of the deformation caused by feeding flies the intestinal irritant dextran sodium sulfate (DSS) (Amcheslavsky et al., 2009), a polyanionic derivative of the polysaccharide dextran. Stemming from this observed similarity, this study investigates whether and how DSS damages the basement membrane, and whether and how crosslinking is important for basement membrane repair. In this report, we introduce a new DSS-based experimental model to probe basement membrane damage and repair, one which is reproducible and suited to microscopy. Using this model, we determine that replacement and crosslinking are essential processes of basement membrane repair.

RESULTS

DSS feeding phenocopies loss of basement membrane proteins in the midgut

We focused on DSS as a potential basement membrane damaging agent. DSS is a 36–50 kDa negatively charged derivative of the carbohydrate polymer dextran, and administering DSS to mice in drinking water has long been used to induce a condition like ulcerative colitis. Because of its use in damaging the mouse intestine, DSS has also been utilized in adult *Drosophila* to damage the fly gut epithelium (Amcheslavsky et al., 2009; Ren et al., 2010, 2013; Karpowicz et al., 2010; Cordero et al., 2012; Tian and Jiang, 2014; You et al., 2014; Tian et al., 2015). In the first report of treating flies with DSS (Amcheslavsky et al., 2009), it was noted that DSS appeared to alter basement membrane around the gut. The basement membrane is a sheet-like extracellular matrix that gets its mechanical strength from covalent crosslinking of the Collagen IV polymer (Bhave et al., 2017). The DSS-induced basement membrane phenotype reported by Amcheslavsky et al. (2009) appeared similar to a phenotype we reported in larvae when we mutated or inhibited Peroxidasin (Pxn), a Collagen IV crosslinking enzyme (McCall et al., 2014). Thus, it seemed possible that DSS was interfering with Collagen IV function.

To examine these similar phenotypes, we compared the treatments of DSS-feeding and ubiquitous *Pxn* knockdown (using *TubP-Gal4*) in the midguts of adult females, which are larger than the midguts of males. The *Drosophila* gut comprises an epithelial monolayer, exposed to the lumen on its apical side and abutting the basement membrane on its basal side. Several basement membranes are expected to lie in close apposition outside the midgut. The epithelial basement membrane lies between the epithelial cells and the underlying visceral muscles responsible for peristalsis, which run circumferentially and longitudinally along the gut. Typically, muscles are wrapped in basement membrane (Yurchenco, 2011). Further, basement membranes separate organs from the body cavity and hemolymph. Fig. 1A shows a schematic of these tissues and their associated basement membranes, based on our imaging in this study.

To visualize the basement membrane, we used *viking* (*vkg*)-*GFP*^{454} (Vkg–GFP hereafter), which has a fully-functional GFP-trapped Collagen IV α2 protein transcribed from the endogenous genomic locus. In these flies, Collagen IV can be easily visualized by GFP fluorescence with standard epifluorescence microscopy (Fig. 1B). We fed flies 3% DSS in a 5% sucrose solution over the course of 2 days and confirmed the previous findings that the tissue appeared altered compared to controls fed only sucrose (Fig. 1B,C; Fig. S1). On closer inspection, we found that the obvious DSS-induced morphological changes were caused by the peristalsis muscles, which appeared as dark areas surrounded by basement membrane. In optical cross-sections along the long axis of the midgut after DSS treatment, the circumferential muscles appeared contracted inward, protruding toward the epithelia and lumen, giving a rounder appearance in cross-section that was also evident by phalloidin staining of actin (Fig. 1E–F′). A similar rounding of circumferential muscles was observed when *Pxn* was knocked down ubiquitously in adults (Fig. 1D). This rounded muscle phenotype was quantified by measuring the aspect ratio of the circumferential muscles in cross-section (Fig. 1D′), which was significantly different from controls (Fig. 1G). The altered appearance of the basement membrane and contracted morphology of the muscles was also evident when we visualized the basement membrane components Laminin (LanB1–GFP; Fig. 1H,I) or Perlecan (Trol–GFP; Fig. 1J,K).

As demonstrated by *Pxn* knockdown, defects in muscle morphology can result from the loss of basement membrane function. A mechanistic relationship between basement membrane function and muscle morphology and function has arisen from muscular dystrophy studies. Normally, muscle contraction force is resisted by the basement membrane, as the contraction force is transmitted by covalent linkages connecting the contractile machinery to the basement membrane (schematic in Fig. 2A). The genes that are defective in muscular dystrophy disease encode proteins comprising components of these mechanical linkages, including the basement membrane protein laminin (Mercuri and Muntoni, 2013). In muscular dystrophy patients, these linkages are disrupted so that muscle-generated contractile forces pull on the unsupported plasma membrane, resulting in membrane tears, calcium entry, muscle hypercontraction and eventual muscle

Journal of Cell Science (2019) 132, jcs226860. doi:10.1242/jcs.226860

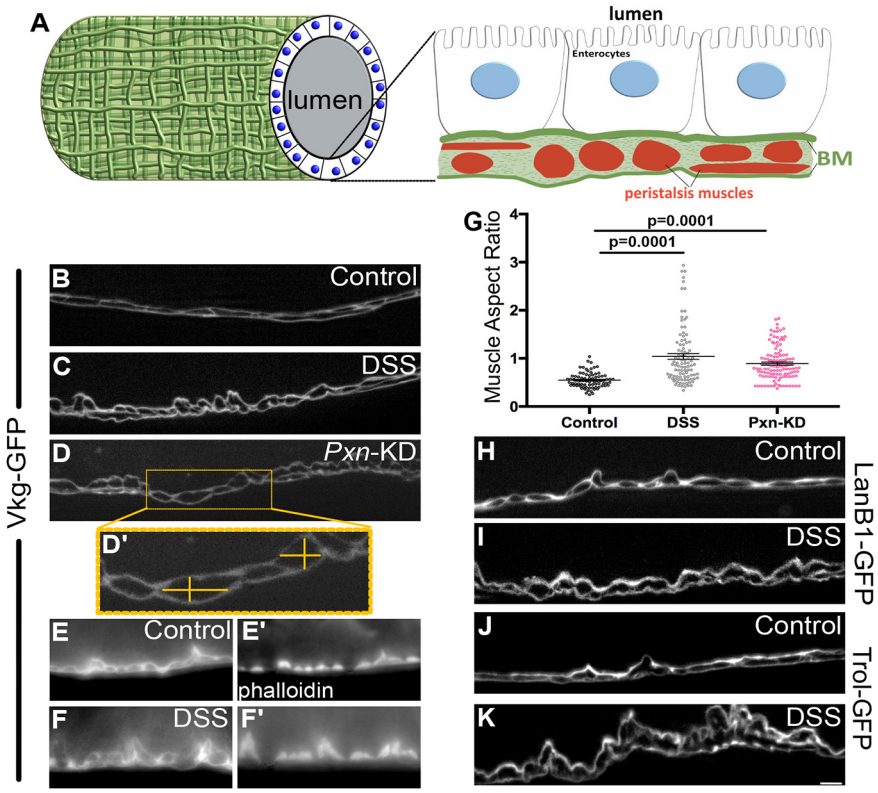

Fig. 1. DSS alters gut muscle morphology, similar to loss of *Pxn*. (A) Schematic representation of the *Drosophila* gut based on imaging in this study. See also Figs S1, S3. (B–D′) A functional Vkg–GFP (Collagen IV α2) protein allows visualization of the basement membrane under the enterocytes and surrounding the muscles. (B) Basement membrane under control conditions. (C) Morphology is disrupted in DSS-fed adult wild-type flies. (D) Morphology is similarly disrupted in flies with adult-onset knockdown of *Pxn* (*Pxn*-KD), a basement membrane cross-linking enzyme, knocked down ubiquitously using *TubP-Gal4*. Muscle aspect ratio measurements are illustrated in D′. (E–F′) Basement membrane labeled with Vkg–GFP (E,F) surrounds muscles stained with phalloidin (E′,F′). After DSS feeding, apparent displacement of basement membrane represents changes in muscle morphology (F,F′). (G) Muscle aspect ratio, measured as in D′, changes in response to either DSS feeding or *Pxn* knockdown. Five to six flies were analyzed for each condition. Data shows mean±s.e.m. *P*-values calculated by ANOVA to determine significance followed by unpaired *t*-tests with Bonferroni correction. (H,I) A functional LanB1–GFP labels basement membrane under the enterocytes and surrounding the muscles. LanB1–GFP-expressing flies fed DSS recapitulate changes in muscle morphology visualized with Vkg–GFP. (J,K) A functional Trol–GFP labels basement membrane under the enterocytes and surrounding the muscles. Trol–GFP-expressing flies fed DSS recapitulate changes in muscle morphology visualized with Vkg–GFP and LanB1–GFP. B–F,H–K are optical cross sections, as illustrated in A. Scale bar: 5 µm.

damage (Nyström et al., 2017; Vila et al., 2017). The visceral muscles in *Drosophila* are striated and multinucleate, more similar to mammalian skeletal muscle than mammalian visceral smooth muscles. Striations are caused by repeating sarcomeres, units of actomyosin contractile machinery, which have multi-protein covalent linkages extending from the Z-bands to the basement membrane (Maartens and Brown, 2015). Previous work has shown that the reduction of Laminin in *Drosophila* ovarian muscles decreases sarcomere size, recapitulating a muscular dystrophy phenotype (Andersen and Horne-Badovinac, 2016). As in ovarian muscles, *Drosophila* gut muscles decreased sarcomere size by about 10% upon reduction of Laminin (*LanB1*-RNAi driven by *TubP-Gal4, Gal80^{ts}*; Fig. 2B–D). We reasoned that if DSS damaged muscles indirectly via the basement membrane, DSS should also decrease sarcomere size. In the DSS-fed flies, an even more pronounced decrease in sarcomere size was observed (∼30%; Fig. 2E–G), although incomplete knockdown of Laminin may have contributed to the bigger effect of DSS. To test whether sarcomere size was reduced by active contraction, we treated guts with relaxation buffer *ex vivo*. Although treatment with relaxation buffer did somewhat increase sarcomere size of both DSS- and control-fed flies, the DSS-treated sarcomeres remained significantly shorter than controls (Fig. S2). Thus the decrease in sarcomere size in DSS-treated guts was not caused by DSS-induced contraction. These results are consistent with the interpretation that DSS damages the basement membrane of peristalsis muscles, leading to muscle damage and altered muscle morphology.

DSS expands the basement membrane sheet

Basement membranes have traditionally been imaged by electron microscopy, so we used transmission electron microscopy (TEM) to image the gut in cross sections perpendicular to the long axis of the gut. In control samples, basement membrane was observed on the basal surface of the enterocytes and also on the outer surface of the muscles; between these layers and in the inter-muscle regions, the organization of the extracellular matrix was unclear (Fig. 3A,A′; Fig. S3). After DSS feeding, the most obvious change to the tissue was in the peristalsis muscles, which were irregular and shredded (Fig. 3B,B′, yellow arrows), consistent with our epifluorescence analysis. Importantly, the basement membrane itself appeared thicker after DSS feeding. Measuring the expansion of the basement membrane on the basal surface of the enterocytes (pseudo-colored green, Fig. 3A′–B′), the basement membrane was 140±60 nm (mean±s.e.m.) thick in controls, whereas after DSS treatment it was 330±250 nm thick (Fig. 3C). Thus, by TEM, the gut peristalsis muscle basement membrane appeared more than twice as expanded in flies fed DSS than in control flies.

Journal of Cell Science (2019) 132, jcs226860. doi:10.1242/jcs.226860

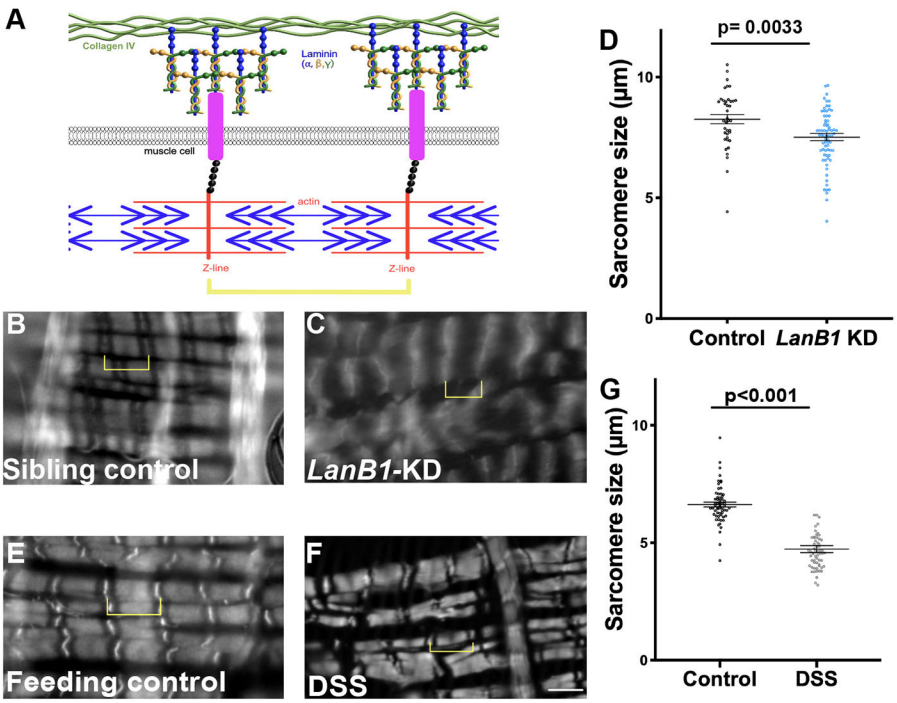

Fig. 2. DSS-induced muscle damage is similar to muscle damage from loss of basement membrane. (A) Schematic representation of the linkage between the actomyosin contractile machinery and the basement membrane. The linkage between the basement membrane and the muscles can occur through integrins or dystroglycans. (B,C,E,F) Phalloidin staining revealed sarcomeres in longitudinal gut muscles. Yellow brackets indicate sarcomeres. Scale bar: 5 µm. (D) Knockdown of *LanB1* (*LanB1*-KD) ubiquitously using *TubP-Gal4* reduced sarcomere size ∼10% compared to control. Sarcomeres were measured in five flies for each condition. (G) Feeding flies DSS reduced sarcomere size ∼30% compared to control. Sarcomeres were measured in four control and six DSS-fed flies. See also Fig. S2 for sarcomere length in relaxing buffer. Data in D,G show mean±s.e.m. *P*-values calculated by unpaired *t*-test.

We were concerned about possible dehydration artifacts associated with fixing samples for EM, and we were also unsure how to interpret the uncharacterized matrix between the apparent basement membrane and the muscles. Thus, we repeated our experiments using super-resolution structured illumination microscopy (SIM), which gave ∼2× increase in resolution compared to diffraction-limited techniques such as laser-scanning confocal (Gustafsson et al., 2008) with two advantages over TEM: a

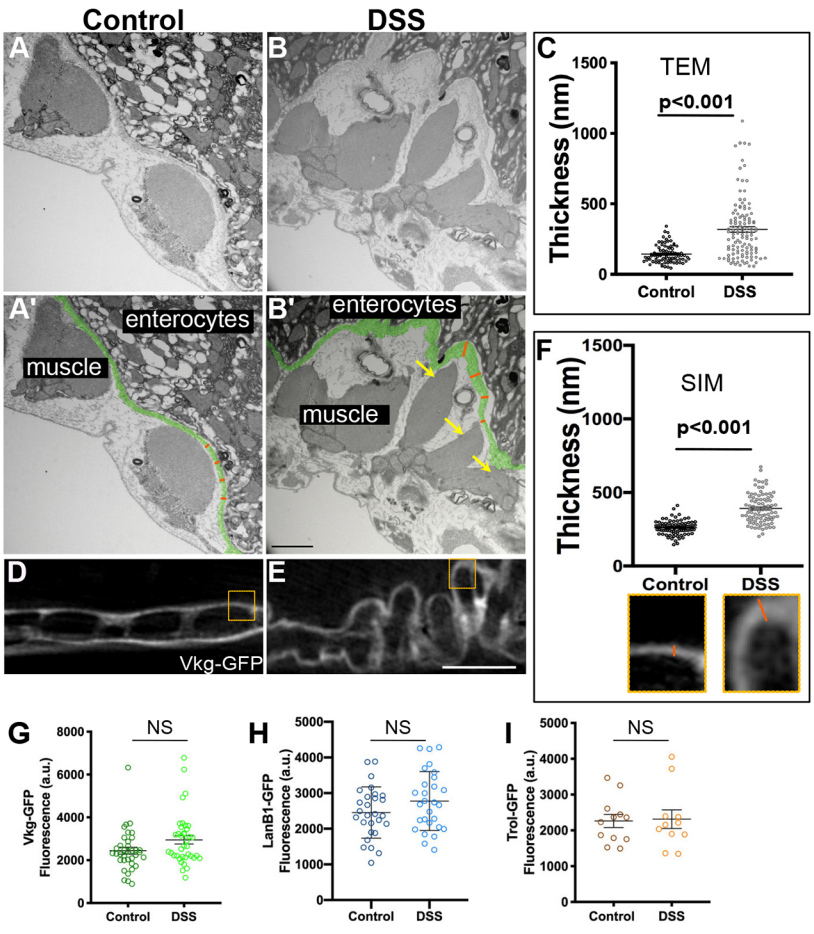

Fig. 3. DSS expands gut basement membrane without changing matrix protein levels. (A,B) TEM images showing the peristalsis muscles and basement membrane of the midgut of a control or DSS-fed fly. (A′,B′) Same images as in A, B with labels. Basement membrane is pseudo-colored green. Orange lines illustrate how basement membrane thickness under the enterocytes (as shown in C) was measured at regular intervals; actual measurements extended across the entire micrograph but orange lines are confined to one region for illustration. Yellow arrows in B′ indicate shredded muscle. Scale bar: 1 µm. (C) Quantification shows a significant increase in the thickness of the basement membrane after DSS feeding. (D,E) Structured illumination microscopy (SIM, super-resolution) images of Vkg–GFP in the midgut basement membrane in control (D) or DSS-fed (E) flies. Scale bar: 5 µm. (F) Quantification shows a significant increase in the thickness of the Vkg–GFP-labeled basement membrane after DSS feeding, measured in a blinded fashion as in insets below *x*-axis, corresponding to boxes in D,E. Measurements were made on four control and five DSS-fed flies. (G–I) Basement membrane protein levels are not significantly different in control versus DSS-fed fly midguts, as indicated by fluorescence levels of Vkg–GFP (G), LanB1–GFP (H) or Trol–GFP (I). Each dot represents one midgut. Data in C,F,G–I show mean±s.e.m. *P*-values calculated by unpaired *t*-test. NS, not significant.

Journal of Cell Science (2019) 132, jcs226860. doi:10.1242/jcs.226860

standard formaldehyde-based immunohistochemistry fixation protocol was utilized, and the basement membrane was identified with fluorescent Vkg–GFP labelling rather than as an unlabeled electron-dense structure. By SIM imaging, the control basement membrane was 260±50 nm thick, whereas DSS-treated basement membrane expanded to 390±100 nm thick (Fig. 3D–F). Thus, two independent fixation and visualization techniques determined that basement membranes expanded after DSS treatment.

Basement membrane expansion could indicate an increase in levels of basement membrane proteins, resulting in a thicker structure; alternatively, it could indicate a fracturing or delaminating mechanical failure of the basement membrane sheet. To address whether increased levels of basement membrane proteins were present after DSS feeding, we measured the total fluorescence of the GFP-labeled basement membrane proteins within the basement membrane around the gut. We imaged the fluorescence of Vkg–GFP (Fig. 3G), LanB1–GFP (Fig. 3H) and Trol–GFP (Fig. 3I), all functional GFP fusions expressed from endogenous regulatory sequences. For each, the total fluorescence levels were unchanged after DSS feeding. Independently, we found no difference in gut length or diameter after DSS feeding (Fig. S4). We conclude that the expansion in basement membrane is not caused by an increase in basement membrane deposition; rather, the basement membrane expansion suggests mechanical failure.

DSS localizes to basement membranes

To gain insight into how DSS expands the basement membrane, we fed fluorescently-labeled FITC–DSS to flies and visualized its localization in unfixed gut tissue after a 6-h chase (Fig. 4A–F). For controls, we fed flies unconjugated FITC (no DSS treatment), or we fed flies unconjugated FITC and unconjugated DSS, as separate molecules, to control for any stickiness of FITC to DSS-damaged tissues (Fig. 4A–C). Basement membrane was labeled with a functional protein-trapped Trol–RFP, rendering the basement

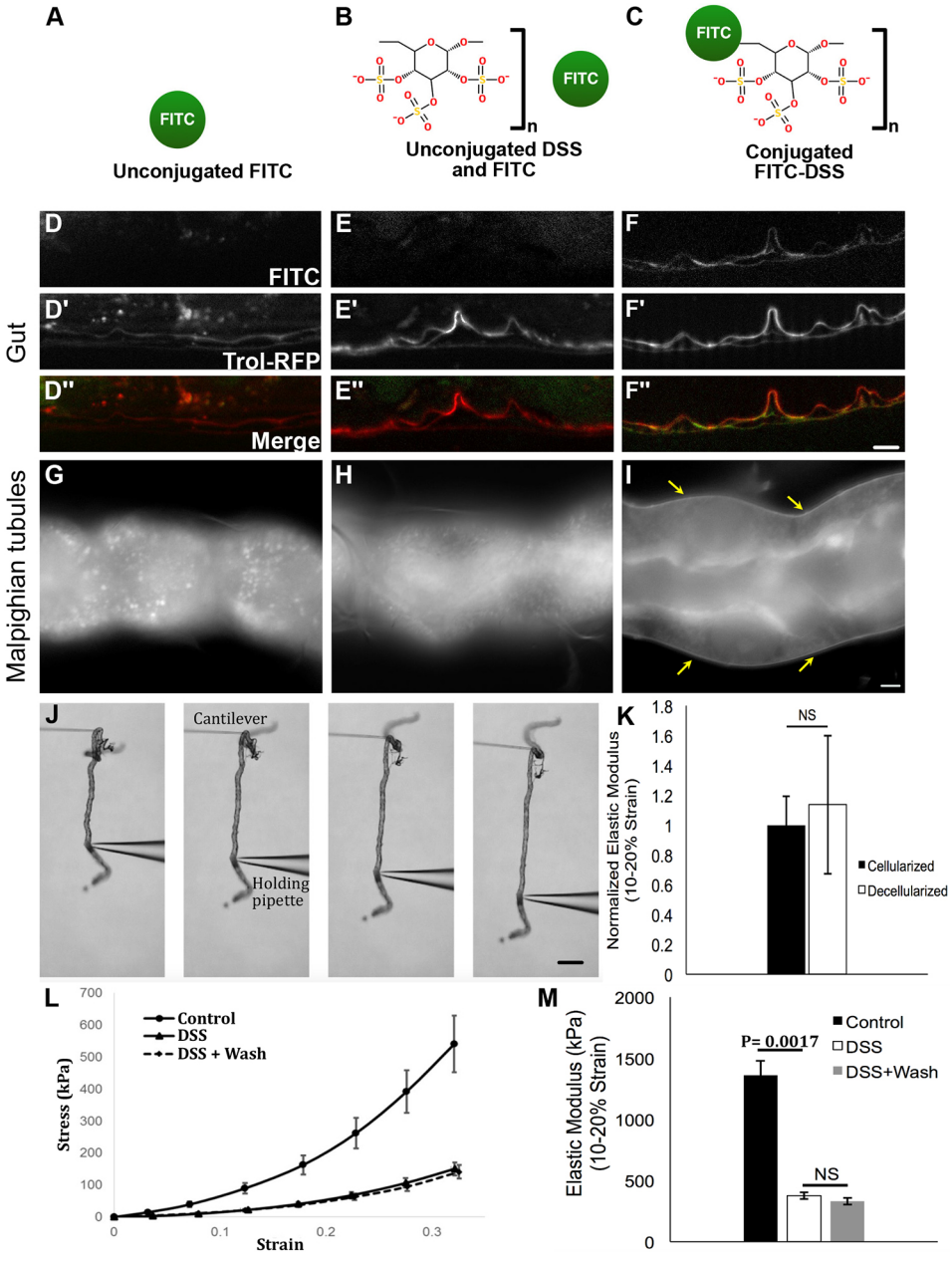

Fig. 4. DSS accumulates in basement membranes where it irreversibly decreases basement membrane stiffness. (A–C) Feeding conditions for testing DSS localization. (D–F″) After feeding, FITC–DSS specifically localizes to the basement membrane, labeled with Trol–RFP, in the midgut. Feeding regimens in D–F″ match the corresponding schematics above in A–C. (G–I) FITC–DSS specifically localizes to the basement membrane (arrows in I) of the Malpighian tubules after soaking *ex vivo*. Soaking regimens in G–I match the corresponding schematics above in A–C. (J) Assay for measuring tubule stress-strain response. The tubule is stretched between a cantilever and a holding pipette. Stress and strain are calculated from the bending of the cantilever and the changes in the tubule length. (K) Normalized stiffness for intact and detergent-decellularized tubules. There was no significant difference between cellularized and decellularized tubules, indicating that resistance to strain is imparted by the basement membrane. Five cellularized and three decellularized tubules were analyzed. (L) Stress-strain curves for control, DSS-treated, and DSS-treated and washed tubules showing a downward shift in the stress-strain curves for DSS-treated tubules. Five flies were analyzed for each condition. (M) Elastic modulus for control and DSS treated tubules, calculated from the data in L. DSS treatment significantly reduced basement membrane stiffness. No significant difference was detected between DSS-treated tubules following removal of DSS (wash). Scale bars: 5 µm in F″, I; 200 µm in J. Data in K–M show mean±s.d. *P*-values calculated by unpaired *t*-test (K) or ANOVA followed by unpaired *t*-tests with Bonferroni correction (M). NS, not significant.

Journal of Cell Science

Journal of Cell Science (2019) 132, jcs226860. doi:10.1242/jcs.226860

membrane red. Labeled FITC–DSS localized reproducibly to the basement membrane of the damaged guts, whereas no fluorescence was observed in the basement membrane of either control (Fig. 4D–F″). These results were obtained in unfixed tissue, as FITC–DSS washed out during the fixation procedure because it has no amine groups to fix it in place. The localization of FITC–DSS to the basement membrane indicates that DSS is transported from the gut lumen through the enterocytes (cells that specialize in nutrient transport) to the adjacent basement membrane where it accumulates; indeed, punctae of FITC–DSS were observed within the epithelial layer (Fig. S5I). The basement membrane morphological expansion could be caused by negatively charged DSS creating osmotic pressure, leading to swelling. This pathological swelling of basement membrane could cause mechanical weakening, as implied by the presence of dysmorphic muscles. Because DSS has been used extensively in mouse models, we performed a similar experiment, feeding FITC–DSS to mice and examining its intestinal localization. In mice, FITC–DSS localizes to punctae along the epithelial layer, co-localizing with intercellular junctions, and not to the underlying basement membrane (Fig. S5), indicating that murine enterocytes do not transport DSS across the epithelial barrier as do *Drosophila* enterocytes.

DSS decreases the mechanical stiffness of basement membranes

We wanted to directly test the stiffness of the basement membrane after DSS treatment; however, the gut basement membrane cannot be separated from the peristalsis muscles, which would significantly alter tissue stiffness independently of the basement membrane. As an alternative, we analyzed the Malpighian tubules, part of the *Drosophila* excretory system. These simple tubules have only a tube-shaped epithelial monolayer surrounded on the outside by basement membrane, without muscle or exoskeleton. We did not expect DSS to diffuse to the Malpighian tubules at high levels after feeding *in vivo* because it gets trapped around the gut; instead, we treated the Malpighian tubules with DSS *ex vivo* by soaking them in a DSS solution for 20 min. As observed for guts after DSS feeding, conjugated FITC–DSS accumulates in the basement membrane surrounding the tubule, whereas unconjugated FITC does not, either in the presence or absence of DSS (Fig. 4G–I).

To measure the stiffness of the Malpighian tubule basement membrane directly *ex vivo*, we used a glass micro-cantilever system to measure the tensile stress-strain response (Fig. 4J). This technique is used to estimate the stiffness of the basement membrane, reported as the elastic modulus (Young's modulus). To evaluate the contribution of the basement membrane to tubule stiffness, we compared the elastic modulus of intact tubules to those that were decellularized by the addition of detergent after dissection. Decellularization did not significantly change the stiffness of the tissue (Fig. 4K), confirming that we were measuring the stiffness of the basement membrane. In contrast, the Malpighian tubule stiffness was significantly decreased after soaking in DSS (Fig. 4L,M), indicating that DSS disrupts the mechanical properties of the basement membrane. We considered the possibility that basement membrane stiffness was altered by DSS only during the time that DSS resided in it, asking whether the stiffness returned immediately upon DSS wash-out. To test this possibility, we used labeled FITC–DSS to determine conditions for washing out DSS after it became lodged in the basement membrane, and then tested Malpighian tubules soaked in DSS and then washed. We found that the elastic modulus of the basement membrane was virtually unchanged after DSS removal (Fig. 4L,M). Thus, *ex vivo* DSS inflicts irreversible mechanical damage on the basement membrane.

One possibility for how DSS could access the basement membrane *in vivo* is by damaging the enterocyte barrier, thus exposing the basement membrane to the contents of the gut lumen including DSS. If this were the case, loss of gut epithelial barrier function would precede or be simultaneous with basement membrane damage. Epithelial barrier function can be evaluated using a blue food dye, which spreads throughout the body of the fly when the intestinal barrier is breached, termed a 'smurf' phenotype (Rera et al., 2011) (Fig. 5A). To investigate the function and loss of the intestinal epithelial barrier, we fed flies with blue dye for 6 days, with or without DSS, and scored the flies regularly for body color (Fig. 5B,C). Dead flies with blue bodies were excluded from the count, as barrier integrity is always lost on death; dead flies were much more prevalent with DSS feeding than without (Fig. 5D,E; Fig. S6). The majority of smurf (blue) flies were observed after 5 days, with the first instance recorded after 3 days, well after the onset of basement membrane damage, assayed after 2 days of DSS feeding when all samples show the effects. Therefore, DSS damages basement membranes directly, rather than after the loss of epithelial barrier.

Basement membranes are repaired 48 h after DSS withdrawal

Taken together, the above data indicate that on feeding, DSS accumulates in the basement membrane of the gut and mechanically damages it, causing the gut muscles to become

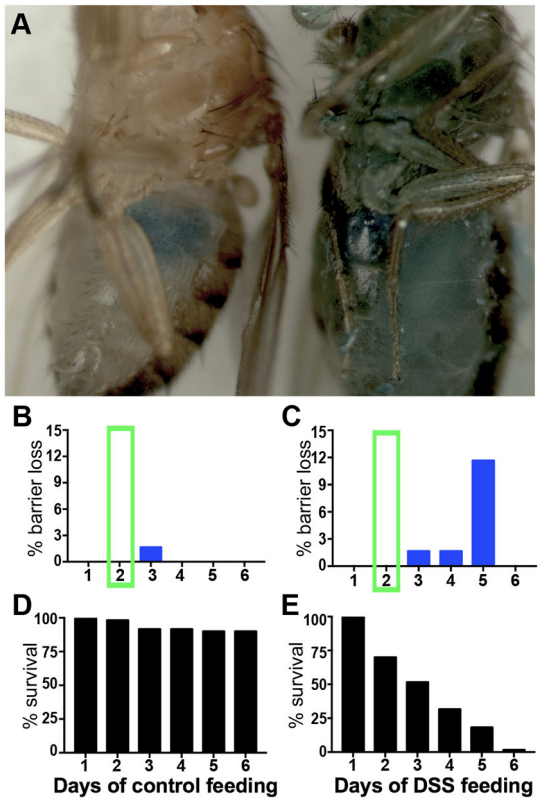

Fig. 5. Basement membrane damage precedes loss of epithelial barrier integrity. (A) In control-fed fly (left), blue dye remained in the gut. In DSS-fed fly (right), the gut lost barrier integrity and blue dye escaped to the body. (B,C) Percentage of living control (B) and DSS-fed (C) flies that lost barrier integrity. Green box highlights 2-day timepoint when basement membrane damage was observed by EM, SIM and muscle morphology. (D,E) Survival of the same flies as in B,C over the course of 6 days on the liquid feeding regimen. 60 flies per condition.

Journal of Cell Science (2019) 132, jcs226860. doi:10.1242/jcs.226860

dysmorphic. Although this damage is irreversible *ex vivo*, we asked whether the basement membrane could be repaired after DSS damage was inflicted *in vivo*. The muscle aspect ratio was surveyed at various times after transferring the flies from DSS treatment back to normal food. Although there was a short-lived reversal of muscle shape within 3 h, lasting recovery was accomplished more slowly, returning to normal 48 h after termination of DSS feeding (Fig. 6A). To confirm that the basement membrane itself had repaired in addition to the muscles, we examined the basement membrane by TEM at 48 h after terminating DSS feeding and found that the basement membrane sheet had returned to its previous undamaged width (Fig. 6B–E). When analyzed by SIM as well as by TEM, the basement membrane of control flies returned to its normal width by 48 h after termination of DSS (Fig. 7G). At 48 h after DSS termination, the levels of basement membrane proteins Vkg, LanB1 and Trol were not significantly different than in undamaged midguts as measured by GFP-fusion protein fluorescence (Fig. S7). Thus, both muscle morphology and direct measurement indicated that basement membrane repaired within two days of DSS treatment withdrawal.

Matrix replacement and collagen crosslinking are required for basement membrane repair

Having established the time course for repair, we analyzed biological requirements for repair. The role of Collagen IV crosslinking in repair was investigated by knocking down the NC1-crosslinking enzyme Pxn ubiquitously in adults using *TubP-Gal4, Gal80^{ts}* for 7 days before feeding with DSS for two days, then removing from DSS to allow repair for two more days. When

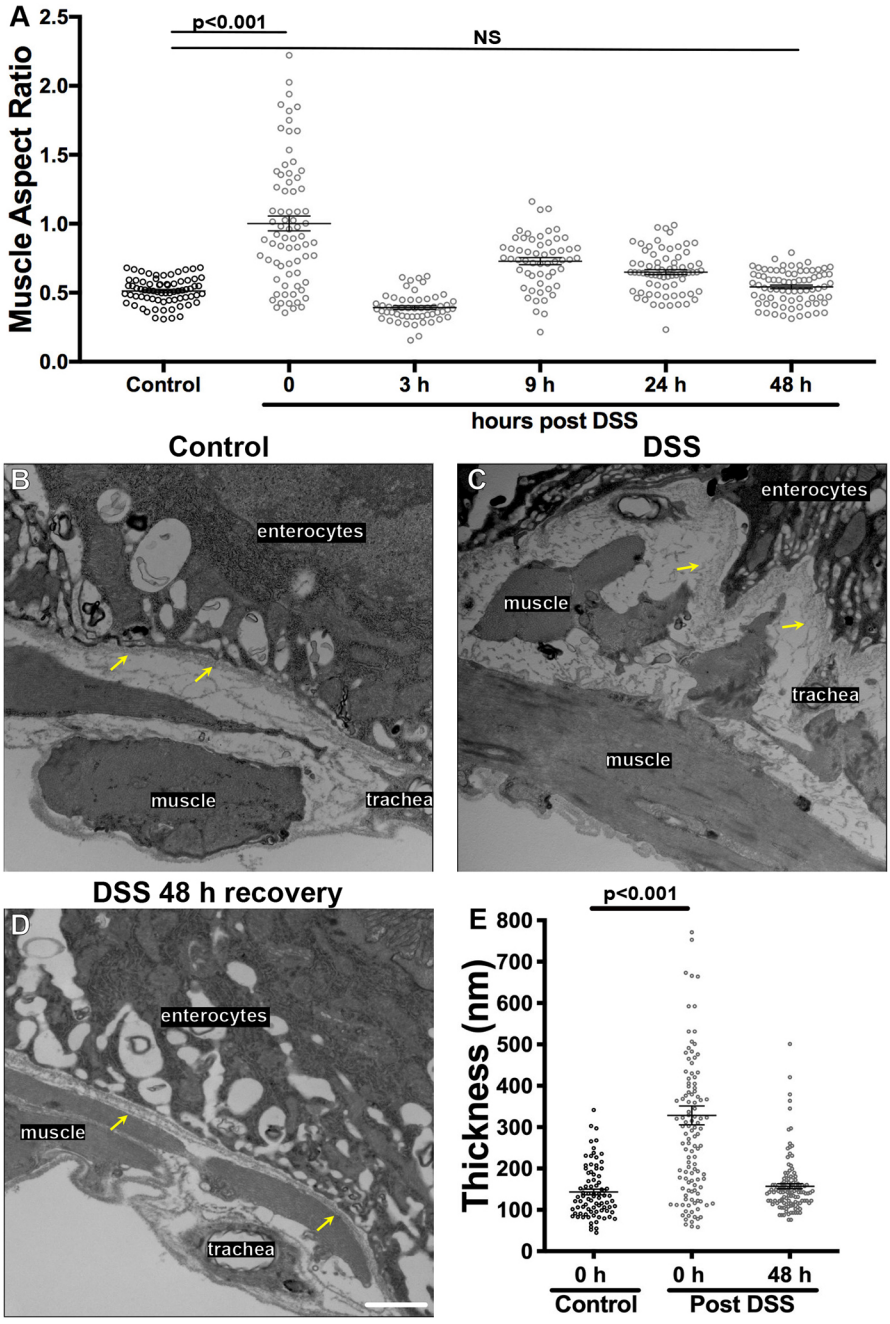

Fig. 6. Basement membrane is repaired 48 h after termination of DSS feeding. (A) Muscle morphology was analyzed at the indicated times after withdrawing animals from DSS food to normal food. The muscle aspect ratio was restored at 48 h after terminating DSS feeding. Four to eight flies were analyzed for each time point. (B–D) TEM image of muscles and basement membrane of the midguts in a control-fed fly (A), DSS-fed fly (B), and a fly that recovered on normal food for 48 h after DSS feeding (C). Basement membranes are indicated with yellow arrows. Both muscle morphology and basement membrane thickness have been repaired by 48 h after termination of DSS feeding. (E) Quantification showing repair of basement membrane thickness 48 h after termination of DSS feeding, measured on TEM micrographs. Scale bar: 1 µm. Data in A,E show mean±s.e.m. *P*-values calculated by ANOVA to determine significance followed by unpaired *t*-tests with Bonferroni correction. NS, not significant.

Journal of Cell Science (2019) 132, jcs226860. doi:10.1242/jcs.226860

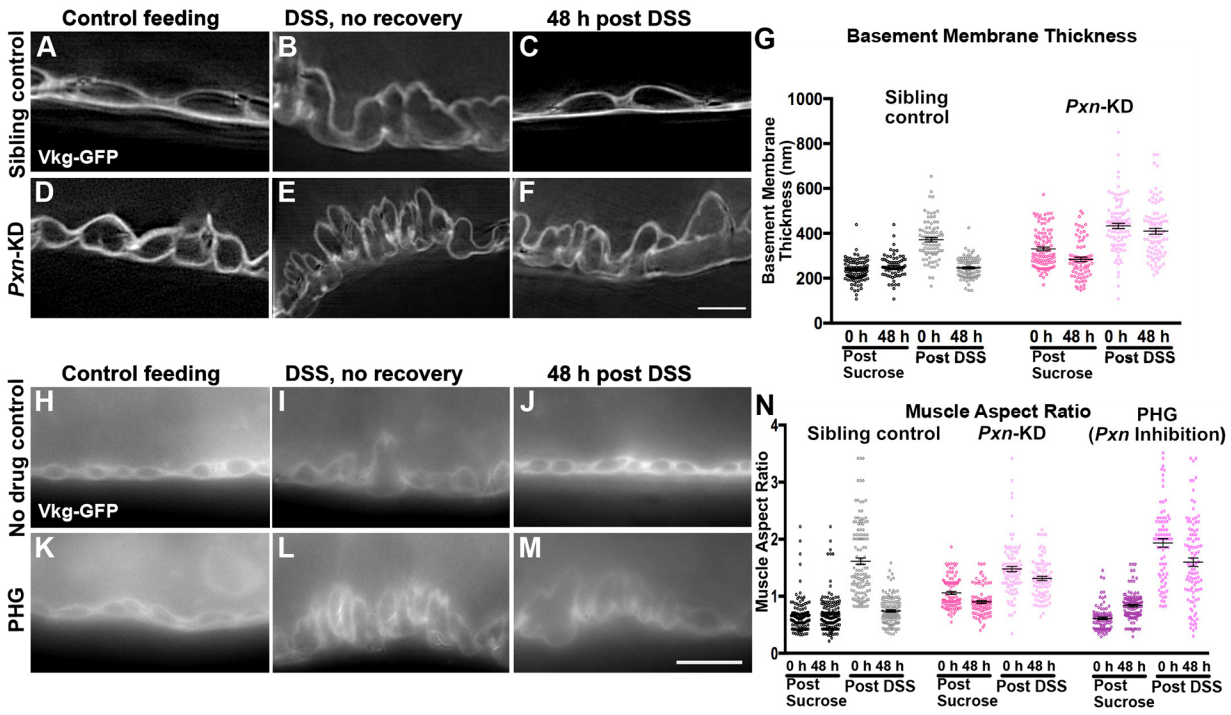

Fig. 7. Peroxidasin is required for basement membrane repair. (A–F) SIM images of Vkg–GFP in the midgut basement membrane of control flies (A–C) or flies with *Pxn* knocked down (*Pxn*-KD) in adults using *TubP-Gal4, Gal80ts*. Basement membrane was thicker upon DSS feeding (B,E) but 48 h after termination of DSS treatment, basement membrane returned to its undamaged thickness in control flies (C) but not *Pxn*-KD flies (F). Repair was also deficient with a second *Pxn* RNAi line (not shown). Scale bar: 5 µm. (G) Quantification of the basement membrane thickness in SIM micrographs. Five to seven flies were analyzed for each condition. (H–M) Epifluorescence images of Vkg–GFP outlining muscles in midguts of no-drug control flies (H–J) or flies fed the Pxn inhibitor PHG (K–M). Muscles become dysmorphic with DSS feeding (I,L), but 48 h after DSS withdrawal muscles return to their undamaged state in control flies (J) but not Pxn-inhibited flies (M). Scale bar: 10 µm. (N) Quantification of the muscle aspect ratio. Four to six flies were analyzed for each condition. Data in G,N show mean±s.e.m. For statistical analysis of significance, see Tables S1 and S2.

basement membrane morphology was analyzed by SIM, the basement membranes of *Pxn*-knockdown flies did not recover and remained expanded even 48 h after they were removed from DSS to normal food, in contrast to sibling controls, in which basement membranes repaired (Fig. 7A–G). We next analyzed muscle aspect ratio as a readout of basement membrane repair in these *Pxn*-knockdown flies. As noted in Fig. 1, even before DSS feeding, the *Pxn*-knockdown muscles have an increased aspect ratio; this ratio is exacerbated by DSS feeding, and it does not recover after removal of DSS (Fig. 7N); we confirmed the specificity of this phenotype with a second *Pxn* RNAi line (not shown). As an independent method of assessing the role of crosslinking, we fed flies phloroglucinol (PHG), an irreversible chemical inhibitor of Pxn (Bhave et al., 2012). PHG has two advantages over genetic knockdown: first, there is no pre-treatment because it is immediately effective, eliminating complications from long-term loss of Pxn before DSS feeding; second, it is likely to give a more penetrant phenotype than RNAi-based knockdown, which is usually incomplete. PHG was administered with the DSS or vehicle, and it caused a modest increase in muscle aspect ratio even without DSS during the course of the 4-day experiment (2 days treatment, 2 days recovery); when combined with DSS, the muscle aspect ratio became severely increased, and this ratio did not recover even 48 h after DSS withdrawal when PHG was maintained in the food (Fig. 7H–N). We conclude that crosslinking is required for repairing the basement membrane after DSS-induced mechanical damage.

We considered two mechanisms by which collagen crosslinking could be required for repair. First, crosslinking might be increased to stabilize the pre-existing collagen within damaged basement membranes, akin to stapling broken fragments together. Theoretically, up to six sulfilimine crosslinks can bridge every NC1 hexamer, but an average of only 2–4 crosslinks per hexamer is detected in bulk fly and vertebrate tissues (Fig. S8A) (Bhave et al., 2012; McCall et al., 2014). Thus, it seemed possible that crosslinking is increased in response to damage within the basement membrane. Alternatively, crosslinking might be required after the incorporation of new collagen IV that replaces damaged proteins, to maintain the original extent of tissue crosslinking. We evaluated these models both genetically and biochemically. We reasoned that if we knocked down Collagen IV with RNAi, collagen replacement would be reduced; simultaneously, we could feed flies PHG to inhibit Pxn. If crosslinking were required only for the replaced collagen in the basement membrane, then the phenotype would be no worse when both were inhibited together. In contrast, if crosslinking and collagen replacement were separate mechanisms of repairing basement membrane, then the phenotype would be worse when both were inhibited (see model in Fig. S8B). We found that the phenotype of inhibiting both processes was no worse than inhibiting each alone (Fig. S8C), arguing that Pxn is required for maintaining the extent of Collagen IV crosslinking after collagen is replaced during repair. In a separate biochemical experiment, we measured the amount of crosslinking in isolated guts by examining NC1 dimer electrophoretic mobility, which changes with crosslinking status, allowing us to calculate the number of crosslinks per hexamer. We found no significant change before, during, or after DSS treatment, with ∼3.7 crosslinks/hexamer in the gut on average, arguing that Collagen IV does not become hyper-crosslinked in response to basement membrane damage (Fig. S8D,E).

Journal of Cell Science (2019) 132, jcs226860. doi:10.1242/jcs.226860

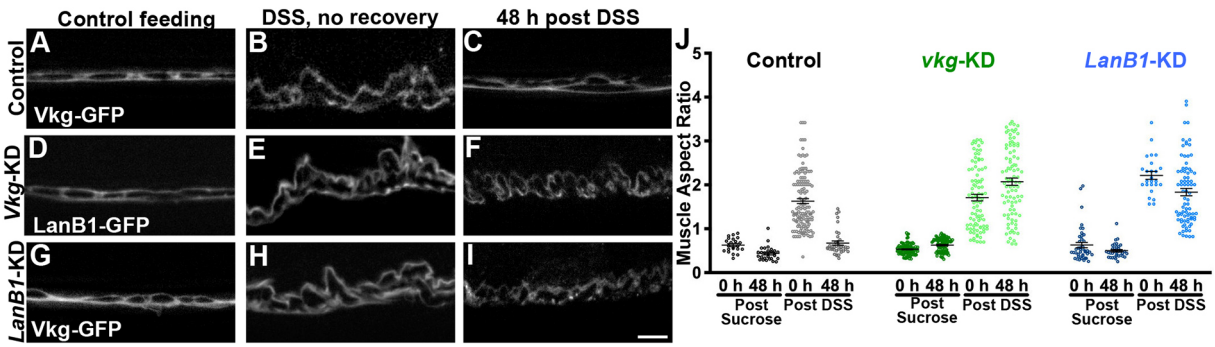

Fig. 8. Basement membrane repair requires new Collagen IV and Laminin. (A–I) Epifluorescence microscopy images of Vkg–GFP (A–C,G–I) or LanB1–GFP (D–F) showing the basement membrane and muscle morphology before, during or after DSS feeding. When *vkg* (*vkg*-KD) or *LanB1* (*LanB1*-KD) is knocked down in adults using *TubP-Gal4, Gal80ts*, basement membranes do not repair as inferred from the muscle morphology (F,I). Scale bar: 10 µm. (J) Quantification of the muscle aspect ratio. Four to six flies were analyzed for all conditions, except three flies for the *LanB1*-KD 48 h sucrose control. Data shows mean±s.e.m. For statistical analysis of significance, see Table S3. The repair-deficient phenotype was observed with second RNAi lines targeting *vkg* or *LanB1* (not shown).

These results indicate that an important mechanism of basement membrane repair is through direct replacement of the matrix components. We tested this model by knocking down two critical components of basement membrane, Collagen IV (*vkg*) and Laminin (*LanB1*), initiating knockdown ubiquitously after the animals reached adulthood. Under the knockdown conditions tested, no effect was observed before damage, but each was required for repairing the basement membrane after damage, as assayed by muscle aspect ratio (Fig. 8). Similar results were observed with second RNAi lines, ruling out off-target effects (not shown). Thus, basement membrane is repaired by replacement and crosslinking of the newly incorporated matrix.

DISCUSSION

DSS damages basement membranes

In this study, we determine that feeding DSS to flies damages the basement membrane around the midgut. Multiple assays were used to reach this conclusion. Specifically, FITC–DSS accumulates in the basement membrane around the midgut after feeding, and FITC–DSS binds to the basement membrane of Malpighian tubules upon soaking. The binding of DSS to basement membrane is relatively weak, as FITC–DSS washes out quickly when either tissue is incubated *ex vivo*. Upon DSS incorporation, the basement membrane expands as measured either by TEM of basement membrane electron density or by super-resolution microscopy of Vkg–GFP. Electron micrographs also show that after DSS incorporation the basement membrane becomes visibly damaged, appearing tattered and less dense. Despite these apparent structural changes, we have not detected changes in the protein composition of the basement membrane, as Laminin, Collagen IV and Perlecan are still present, and the fluorescence levels of Collagen IV, Laminin, and Perlecan GFP protein traps are the same as in undamaged tissue. Basement membrane tensional stiffness is altered upon DSS incorporation into Malpighian tubules, which contain only epithelial cells surrounded by basement membrane, with no other components such as muscles or cuticle to alter their response to tension. The tensional stress-strain assay reveals that DSS irreversibly damages the basement membrane *ex vivo*, rather than temporarily changing stiffness during its incorporation, as the basement membrane does not recover its stiffness after the DSS is washed out. Finally, after removal of DSS from food, repair of basement membrane occurs over 48 h *in vivo*. This repair process requires basement membrane proteins, including Collagen IV, Laminin and the Collagen IV crosslinking enzyme Pxn.

Although DSS clearly damages basement membrane, it is not possible to conclude that DSS damages no other tissue component. Interestingly, mouse enterocytes do not transport DSS across the epithelial barrier and DSS accumulates along extracellular junctions in the mouse intestinal lumen; although DSS is usually administered to mice for 7 days or longer (Chassaing et al., 2014), the level of tight junction protein ZO-1 begins to decrease after one day, with barrier permeability first observed at 3 days (Poritz et al., 2007), which is the same time as the earliest barrier permeability in flies. However, in flies the onset of basement membrane damage occurs before barrier permeability, so basement membrane damage is not secondary to barrier loss. Several lines of evidence support the conclusion that the substantial muscle damage induced by DSS feeding is secondary to basement membrane damage: similar muscle damage is recapitulated by *Pxn* knockdown, muscle morphology is not restored unless new basement membrane proteins can be incorporated, and basement membrane is damaged independently of muscles in the Malpighian tubules. We conclude that DSS causes direct damage to basement membranes, easily assayed by measuring muscle aspect ratio. Damage can also be measured by SIM, EM or mechanical stiffness assays.

Basement membrane repairs within 48 h by replacement and crosslinking

Importantly, upon termination of DSS feeding, the basement membrane around the gut was repaired within 48 h, as assayed by both width measurements and muscle morphology. With repair cleanly separated from damage, DSS represents an excellent system for analysis of basement membrane repair. Feeding adult flies DSS is easy and creates reproducible damage in the gut basement membrane, which can be scaled up for biochemical analysis or genetic screening. The *Drosophila* gut itself is well suited to genetic analysis and microscopy, and unlike mechanical wounding, feeding DSS does not create cellular debris and/or clotting, which can be problematic for imaging. Further, *Drosophila* offers an excellent system for genetic analysis of basement membrane, as it has the same four basic protein components as mammals (Collagen IV, Laminin, Perlecan, and Nidogen) but there are far fewer genes encoding them (Ramos-Lewis and Page-McCaw, 2018) and the enzymes that modify basement membrane are also conserved but fewer in number, with one peroxidasin to promote Collagen IV crosslinking (Soudi et al., 2012) and two matrix metalloproteinases to cleave basement membrane proteins (Page-McCaw et al., 2003). We found some evidence for a fast-acting and temporary stabilization within 3 h of

withdrawing DSS, but this reversal was short-lived; repair was a slower process, leading to a gradual improvement over 48 h.

Using this system, we began an analysis of basement membrane repair. Production of new Laminin and Collagen IV are required for repair, indicating that the basement membrane is repaired through replacement of original matrix components, rather than by crosslinking damaged components or replacing with different proteins. The crosslinking enzyme Pxn is also required. Because of the temporary improvement in aspect ratio observed at 3 h, we asked whether NC1 sulfilimine crosslinking acted independently of protein replacement to stabilize basement membranes, but both biochemical and genetic analysis indicated that the role of Pxn is limited to crosslinking the newly incorporated replacement Collagen IV molecules.

Homeostasis of the gut and its basement membrane

The *Drosophila* gut is a widely used model of stem cell-mediated homeostasis and regeneration. In this self-renewing tissue, cellular repair appears to use the same mechanisms as homeostasis, in that enterocytes and entero-endocrine cells are regularly replaced during adult life. Interestingly, our results show that in the gut basement membrane, *Pxn* is required for both repair of damage and also for basement membrane maintenance. The maintenance requirement suggests that even without damage, there is turnover of either sulfilimine crosslinks or collagen IV during homeostasis, suggesting that the gut basement membrane may be a more dynamic matrix than previously suspected. Similar to what is seen for cellular homeostasis and repair, basement membrane repair may also utilize the same mechanisms as homeostasis.

MATERIALS AND METHODS

Fly husbandry

Drosophila melanogaster stocks were maintained at 25°C on standard cornmeal-molasses food unless otherwise indicated. See Table S4 for a complete description of fly lines used. For the temperature-sensitive RNAi experiments under $Gal80^{ts}$ control, crosses between *Tub-Gal4, Tub-*$Gal80^{ts}$ and *UAS-(gene)*^{RNAi} were performed at 18°C and progeny were allowed to grow to adults at 18°C. 3–5 day old (mated) female flies were then transferred to 29°C for indicated times. For *Pxn* knockdown, adult females remained at 29°C for 14 days before dissection. To minimize basement membrane damage prior to DSS exposure in repair assays, *Pxn* knockdown or *LanB1* knockdown adult females were transferred to 29°C for 7 days prior to DSS/sucrose feeding, whereas *vkg* knockdown flies were transferred to 29°C for 11 days prior to DSS/sucrose feeding.

DSS feeding regimen

As described in Amcheslavsky et al. (2009), a 2.5 cm×3.75 cm piece of chromatography paper (Whatman, 3030-861, Grade: 3 MM CHR) was placed in an empty vial. 500 µl of a 5% sucrose solution with or without 3% 36–50 kDa DSS (dextran sulfate sodium salt colitis grade, MP Biomedicals, CAS number 9011-18-1; 36,0000–50,000 MW) was added directly to the chromatography paper in the vial. Anesthetized flies were carefully added to the vial so as to prevent them contacting the liquid media. Flies were transferred to a new vial with fresh media daily. Flies were fed according to this regimen for 48 h at 29°C. For recovery experiments, flies were allowed to recover for 48 h at 29°C on standard cornmeal molasses food. When indicated, 100 µM phloroglucinol (Sigma-Aldrich, 108736) was added to the DSS or sucrose solution before spotting onto the chromatography paper. For recovery in the presence of phloroglucinol, flies were transferred to molasses food (no cornmeal) containing 100 µM of phloroglucinol in solid media. Cornmeal was excluded to prevent the flies from eating around the phloroglucinol.

Gut dissections and preparation of posterior midguts

Adult females were placed in cold 1× PBS (137 mM NaCl, 2.7 mM KCl, 10 mM Na_2HPO_4, 1.8 mM KH_2PO_4) and were pinched with sharp #5 dissecting forceps (Dumont) between the abdomen and the thorax to separate the abdomen from the rest of the body. The abdominal cuticle was peeled off, leaving the guts and Malpighian tubules. Dissecting guts this way prevents them from being torn or pulled. Guts were dissected and immediately transferred with a Pasteur pipette into a 4% paraformaldehyde (Ted Pella Inc., 18505) in PBS fixative for 10 min at room temperature, and washed 3×5 min with PBS. For SIM analysis and for knockdown experiments in Fig. 8, guts were immunostained for GFP: blocked at 4°C overnight or room temperature for 2 h in blocking buffer (5% BSA, 5% normal goat serum, 0.05% NaN_3), then incubated with rabbit anti-GFP (Torrey Pines, TP401) at 1:200 in blocking buffer for 12 h at 4°C or 2 h at room temperature, then washed 3×10 min at room temperature in PBS, and then incubated with FITC donkey anti-rabbit (Jackson ImmunoResearch, 711-095-152) diluted 1:150 in blocking buffer for 12 h at 4°C or 2 h at room temperature, washed and mounted. When indicated, Alexa Fluor 647-conjugated phalloidin (Life Technologies), diluted 1:20 in blocking buffer, was added to secondary antibodies and incubated overnight at 4°C. All samples were mounted in DAPI-containing mounting media (Vectashield, Vector Laboratories, H1200). Analysis was confined to the posterior midgut, identified by its location anterior to the Malpighian tubules and posterior to the copper cell region, as depicted in the graphical abstract cartoon in Li et al. (2013). For gut dimensions, length was measured on intact guts from the crop to the posterior-most end of the gut; circumference was measured at the thickest part of the posterior midgut region.

Light microscopy

For standard epifluorescence imaging, single optical sections were captured using a Zeiss Apotome mounted to an Axio Imager M2 with a 63×/1.3 oil objective. Images were taken with an AxioCam MRm camera (Zeiss), X-Cite 120Q light source (Excelitas Technologies), and AxioVision 4.8 software (Zeiss). ImageJ (version 1.48v, National Institutes of Health) 16-bit, grayscale, ZVI files were used for image analysis as well as for the images shown. For structured illumination microscopy (SIM), samples were mounted under a #1.0 coverglass (FisherBrand) and imaging and processing were performed on a GE Healthcare DeltaVision OMX equipped with a 60× Plan-apochromat N/1.42 NA oil objective lens and sCMOS camera.

For fluorescence intensity measurements of Vkg–GFP, LanB1–GFP, and Trol–GFP, samples to be compared were prepared on the same day and imaged at the same exposures. For each midgut, a representative field of the posterior midgut was imaged in a single optical cross section with a Nikon Apotome and a 63× objective. Within the field, a region of the midgut was selected for measurement based on its morphology, as only straight regions were analyzed. The ImageJ Measure tool was used to measure the total fluorescence intensity within a standard box (uniform length and area) that enclosed all the basement membrane of the enterocytes and muscles along a straight section of the midgut. An unpaired *t*-test was performed (GraphPad Prism 7.0). As an independent method to verify the fluorescence intensity of Vkg–GFP, we imaged three dimensions of the entire posterior midgut region of 40 sucrose- and 54 DSS-treated guts using a Nikon Spinning Disk microscope (Yokogawa CSU-X1 spinning disk head with Andor DU-897 EMCCD camera). After excluding regions that were out of focus, the maximum-intensity fluorescence projections were measured across the midgut, and data were compared using an unpaired *t*-test (GraphPad Prism 7.0). Like the first method, this second method of determining fluorescence intensity showed no difference between sucrose- and DSS-fed flies.

Transmission electron microscopy

Samples were processed for TEM and imaged in the Vanderbilt Cell Imaging Shared Resource-Research EM facility. Samples were dissected in and fixed with 2.5% glutaraldehyde in 0.1 M cacodylate buffer, pH 7.4 at room temperature for 1 h then left at 4°C for 10 days. The samples were washed 3×5 min in 0.1 M cacodylate buffer, then incubated 1 h in 1% osmium tetroxide at room temperature, then washed with 0.1 M cacodylate buffer (1% calcium chloride, 0.1 M sodium cacodylate, and pH adjusted to 7.4). Subsequently, the samples were dehydrated through a graded ethanol series: 30%, 50%, 75%, 85%, 95%, 100%, 100%, 100% each for 15 min followed by a 1:1 solution of 100% ethanol and propylene oxide (PO) for 5 min. Samples were then infiltrated with 25% Epon 812 resin:75% PO for

35 min at room temperature. Next, they were infiltrated with 50% Epon 812 resin:50% PO for 1 h at room temperature then exchanged with new 50% Epon 812 resin:50% PO and incubated overnight at room temperature. Next day, the samples went through a 75%: 25% (resin: PO) exchange, were then exchanged into pure epoxy resin for 3–4 h, then incubated with pure epoxy resin overnight. Next, the resin was exchanged with freshly made, pure epoxy resin and incubated for 3 h, then embedded in epoxy resin and polymerized at 60°C for 48 h. For sectioning and imaging, 70–80 nm ultra-thin sections were then cut from the block and collected on 300-mesh copper grids. The copper grids were post-section stained at room temperature with 2% uranyl acetate (aqueous) for 15 min and then with Reynold's lead citrate for 10 min. Samples were subsequently imaged on the Philips/FEI Tecnai T12 electron microscope at 6500, 11,000, 15,000, 21,000 and 30,000× magnification.

Basement membrane damage assays

Measurements of basement membrane thickness

Transmission electron microscopy (TEM) images of the basement membrane underlying either the gut epithelial layer or surrounding the Malpighian tubules were acquired at 30,000× magnification and analyzed in ImageJ. Measurements of basement membrane thickness were taken at regular intervals across the field of view from at least 10 images per experimental condition only where the basement membrane was clearly defined. A *t*-test was performed to compare DSS-fed versus sucrose-fed flies, using GraphPad Prism 7.0. Alternatively, SIM was used to measure basement membrane thickness as labeled using Vkg–GFP fluorescence. A rotation student, unfamiliar with the experiment and blinded to sample identity, chose the locations and made the measurements. GraphPad Prism 7.0 was used to perform statistical analysis on the sample set.

Sarcomere measurements

The sarcomere size was measured in gut muscles stained with phalloidin by drawing a line in ImageJ (version 1.48v) from one phalloidin-stained actin region to the next phalloidin-stained actin region. When indicated, guts were dissected in relaxation buffer (20 mM sodium phosphate, 5 mM $MgCl_2$, 5 mM EGTA, 5 mM ATP solution, 5 mM DTT, 10 mM 100× Halt Protease Inhibitor) and allowed to incubate for 30 min before further processing (Xiao et al., 2017).

Measurement of the muscle aspect ratio

To quantify muscle morphology, the aspect ratio (height:width) of the muscles surrounded by basement membrane was determined from the basement membrane staining (Vkg–GFP or LanB1–GFP) surrounding the muscle. Height was measured at the tallest part of the muscle, and a line perpendicular to the height line was measured as the width, as shown in Fig. 1D′. Aspect ratio was calculated as height:width.

Measurement of Malpighian tubule basement membrane stiffness

Malpighian tubule basement membrane stiffness was measured in a similar manner to that described previously (Bhave et al., 2017). Briefly, measurement cantilevers were fabricated from pulled hollow glass capillary tubes and cantilever spring constants were measured in a manner similar to Shimamoto and Kapoor (2012). Malpighian tubules were attached to the measurement cantilever and a holding pipette (10 µm inner diameter), as shown in Fig. 4J, by applying vacuum. Both the measurement cantilever and holding pipettes were attached to micromanipulators. Imaging was performed on an inverted microscope (VWR) at 4× magnification with an attached digital camera for image acquisition. The holding pipette was translated in 40 µm increments to stretch the tubule and deflect the measurement cantilever. Images acquired at each deflection increment were used to calculate the deflection of the measurement cantilever and the displacement of the holding pipette. The change in the length of the tubule (Δl) was calculated as the difference between the distance traveled by the holding pipette and the deflection of the measurement cantilever (d_m). Initial length of the tubule was measured from an image acquired prior to translating the holding pipettes. After the experiment was complete, tubules were observed to return to their original length, indicating that only elastic strain had been recorded.

Stress and strain were calculated according to equations:

$$\alpha = \frac{k_m d_m}{A} \quad (1)$$

$$\varepsilon = \frac{\Delta l}{l_o}, \quad (2)$$

where α is the stress, A is the cross-sectional area of the tubular basement membrane, ε is strain and l_o is the initial tubule length (Bhave et al., 2017; Shimamoto and Kapoor, 2012). Area was calculated from the diameter of the tubule, averaged from six different measurements along its length, and the average width of the basement membrane as measured from TEM imaging.

FITC–DSS treatments

For feeding experiments, 3–5-day-old female flies were fed for 48 h on 5% sucrose/3% DSS, with the DSS prepared as follows: FITC–DSS (Sigma Aldrich, 78331-1G) diluted 1:10 with regular DSS; DSS and unconjugated FITC in the same molar ratio as in the first condition (0.86 mg FITC and 300 mg DSS in 10 ml water); FITC alone at a matched molar concentration. After feeding, flies were placed on normal cornmeal-molasses food for 6 h as a chase, then guts were dissected in PBS and immediately mounted in Grace's insect media (BioWhittaker, 04649F) for imaging without fixation.

For Malpighian tubule soaking experiments, tubules were dissected from 3–5-day-old female flies in PBS and immediately transferred to PBS containing one of the following: either FITC–DSS diluted 1:10 with regular DSS; DSS and unconjugated FITC in the same molar ratio as in the first condition (0.86 mg FITC and 300 mg DSS); or FITC alone at a matched molar concentration. Tubules were soaked for 20 min, then washed 3×2 min each with PBS, and mounted and imaged without fixing in PBS. To wash out the FITC–DSS or control FITC after soaking as above, tubules were washed 5×5 min washes in 1× PBS, which was determined by visual inspection under epifluorescence microscopy as sufficient to remove the fluorescence signal.

For mouse DSS experiments, mouse animal experiments were performed under protocols approved by the Vanderbilt University Animal Care and Use Committee and in accordance with NIH guidelines. C57BL6/J mice (Jackson Laboratory) were administered a 2.5% DSS solution in the drinking water consisting of 10% FITC-conjugated DSS/90% unconjugated DSS and were euthanized 24 h later. Control mice received a mix of 10% FITC+DSS (unconjugated)/90% unconjugated DSS. Upon euthanasia, intestinal tissues were removed, washed with 4% PFA, and spread longitudinally onto Whatman paper. Tissues were swiss-rolled, embedded in optimal cutting temperature medium (OCT), and frozen immediately at −80°C. For microscopy, tissues were sectioned at 5 mm thick onto glass slides. Slides were washed once in PBS and incubated at room temperature overnight in primary antibodies against EpCam (rat monoclonal G8.8, Santa Cruz Biotechnology, 53532) or Laminin (rabbit polyclonal, Sigma-Adrich, L9393) at 1:100 dilution, followed by three washes in PBS, and 1 h incubation in Alexa Fluor 647-labeled secondary antibodies at 1:500 dilution (Life Technologies, donkey anti-rabbit-IgG A31573 or goat anti-rat-IgG A21247) and Hoechst 33342 (Invitrogen, H3570) (1:100). Slides were mounted in Prolong Gold and viewed using fluorescent microscopy.

Gut barrier assay

60 w^{1118} flies were fed with DSS or sucrose as above but also including 0.5% erioglaucine disodium salt (aka Brilliant Blue; Sigma-Aldrich, 861146). The flies were examined three times daily (8:00 am, 2:00 pm, 8:00 pm) to assess barrier integrity (appearing blue or 'smurf' when barrier integrity is lost). The flies were deemed smurf only if their bodies were blue and they were alive. Every smurf fly was dead by the next time point.

Western blotting

Each sample contained roughly 200 w^{1118} adult fly guts, dissected in Grace's insect media. Guts were transferred in 25-gut cohorts into a 2 ml pre-tared tube on ice, repeated until all samples were collected. Media was removed and samples were weighed, as 200 mg was a minimum starting mass. Samples were snap-frozen with liquid N_2. Using a cold mortar and pestle, frozen guts were ground into a fine powder, which was weighed then

refrozen in liquid N_2. Samples were resuspended in deoxycholate solubilization buffer (1% sodium deoxycholate, 10 mM Tris pH 7.4, 1 mM EDTA) with 100× protease inhibitors (Thermo Scientific, 78430) and 50 µM phloroglucinol, at a concentration of 5 µl buffer per mg of powdered guts. Samples were sonicated (1 s pulse separated by 1 s pause for a total of 20 s) then incubated for 15 min on ice. To enrich for Collagen IV, samples were spun in a microfuge at 16.1 ***g*** for 30 min at 4°C, the pellet was washed (1 ml/200 mg sample) with chilled high salt wash (1 M NaCl, 50 mM Tris pH 7.4, 100 µM phloroglucinol), vortexed and incubated on ice for 15 min, then spun at 4°C for 30 min. The pellets were then washed (1 ml/200 mg sample) in a hypotonic wash (10 mM Tris pH 7.4, 50 µM phloroglucinol), tubes were inverted to rinse pellet, and then spun for 5 min at 4°C. Bacterial collagenase [1 mg/ml bacterial collagenase CLSPA (Worthington, LS005273), 5 mM $CaCl_2$, 10 mM Tris pH 7.4, 0.1 mM phloroglucinol, 10 mM 100× Halt Protease Inhibitor] was added to the pellet at a concentration of 1 ml/200 mg sample, and the tube was inverted multiple times before being wrapped in foil and incubated for 24 h in a 37°C water bath. Precipitate was removed by spinning down at 4°C for 30 min, and the supernatant containing the Collagen IV NC1 domains was immediately collected and filtered through a 0.2 µm pore mini-syringe filter. Using a Thermo Scientific NanoDrop 1000 spectrophotometer, the protein amount was determined, then samples were lyophilized and resuspended in water at the standardized concentration of 10 mg/ml. 200 ng of sample was run per lane. Samples were resuspended in non-reducing 4× sample buffer (200 mM Tris-HCl pH 6.8, 8% SDS, 40% glycerol, 0.2% Bromophenol Blue), heated for 5 min at 95°C, and loaded onto a Bio-Rad non-reducing 10% gel (Mini-PROTEAN TGX, 456-1034), and run at 100 volts. After removal from the apparatus and before transfer, the gel was reduced in 1× transfer buffer (25 mM Tris base, 192 mM glycine) with 2% β-mercapthoethanol (Fisher Scientific, 60-24-2) for 1 h at room temperature. A rabbit anti-NC1 primary antibody (1:500; McCall et al., 2014) and a 680 anti-rabbit secondary antibody (1:8000; LI-COR Biosciences, 926-32223) were used for imaging on an Odyssey CLx imaging system (LI-COR Biosciences).

Acknowledgements
We thank A. Scott McCall for his original recognition that *Pxn* loss of function phenocopied DSS treatment. We thank Lauryn Luderman and James O'Connor for assisting with blinded experiments and Dhiraj Peddu for help assessing smurf flies at night. We are grateful to Vincent Mirouse for the generous gift of the Trol–RFP fly line. Fluorescence intensities were measured with the help of Bryan Millis at the Nikon Center of Excellence. Indrayani Waghmare, James O'Connor, and Will Ramos-Lewis were essential for discussions and comments along the way. Electron microscopy was performed in part through the use of the Vanderbilt Cell Imaging Shared Resource (supported by National Institutes of Health grants CA68485, DK20593, DK58404, DK59637 and EY08126). We are grateful to the Bloomington *Drosophila* Stock Center and the Vienna *Drosophila* RNAi Center for fly lines. A huge thank you to A.M.H.'s three fur children: Charles contributed great positivity and excitement, and Megs and Benjamin 'contributed' to editing.

Competing interests
The authors declare no competing or financial interests.

Author contributions
Conceptualization: A.M.H., G.B., A.P.; Methodology: A.M.H., A.M.F., K.S. LaFever, D.T.B., G.B., N.F., A.P.; Validation: A.M.H., K.S LaFever, C.R.S., N.F.; Formal Analysis: A.M.H., G.B., N.F.; Investigation: A.M.H., K.S. LaFever, C.R.S., N.F.; Writing-original draft: A.M.H., N.F., A.P.; Writing-review and editing: A.P.; Supervision: K.S. Lau, D.T.B., A.P.; Project Administration: A.P.; Funding Acquisition: K.S. Lau, D.T.B, G.B., A.P.

Funding
This work was supported by National Institutes of Health grants R21AR072510 to A.P.-M., R35GM125028 to D.T.B., F31HL136081 to A.M.F., R01DK103831 to K.S. Lau, R01DK116964 to G.B., and a Burroughs Wellcome Fund Career Award for Medical Scientists (13030995) to G.B. A.M.H. and C.R.S. were supported by National Institutes of Health training grants T32HD007502 and T32AI007281, respectively. Deposited in PMC for release after 12 months.

Supplementary information
Supplementary information available online at
http://jcs.biologists.org/lookup/doi/10.1242/jcs.226860.supplemental

References
Amcheslavsky, A., Jiang, J. and Ip, Y. T. (2009). Tissue damage-induced intestinal stem cell division in Drosophila. *Cell Stem Cell* **4**, 49-61.
Andersen, D. and Horne-Badovinac, S. (2016). Influence of ovarian muscle contraction and oocyte growth on egg chamber elongation in Drosophila. *Development* **143**, 1375-1387.
Bhave, G., Cummings, C. F., Vanacore, R. M., Kumagai-Cresse, C., Ero-Tolliver, I. A., Rafi, M., Kang, J.-S., Pedchenko, V., Fessler, L. I., Fessler, J. H. et al. (2012). Peroxidasin forms sulfilimine chemical bonds using hypohalous acids in tissue genesis. *Nat. Chem. Biol.* **8**, 784-790.
Bhave, G., Colon, S. and Ferrell, N. (2017). The sulfilimine cross-link of collagen IV contributes to kidney tubular basement membrane stiffness. *Am. J. Physiol. Renal Physiol.* **313**, F596-F602.
Bunt, S., Hooley, C., Hu, N., Scahill, C., Weavers, H. and Skaer, H. (2010). Hemocyte-secreted type IV collagen enhances BMP signaling to guide renal tubule morphogenesis in Drosophila. *Dev. Cell* **19**, 296-306.
Chassaing, B., Aitken, J. D., Malleshappa, M. and Vijay-Kumar, M. (2014). Dextran sulfate sodium (DSS)-induced colitis in mice. *Curr. Protoc. Immunol.* 104, 15.25.1-15.25.14.
Cordero, J. B., Stefanatos, R. K., Scopelliti, A., Vidal, M. and Sansom, O. J. (2012). Inducible progenitor-derived Wingless regulates adult midgut regeneration in Drosophila. *EMBO J.* **31**, 3901-3917.
Cummings, C. F., Pedchenko, V., Brown, K. L., Colon, S., Rafi, M., Jones-Paris, C., Pokydeshava, E., Liu, M., Pastor-Pareja, J. C., Stothers, C. et al. (2016). Extracellular chloride signals collagen IV network assembly during basement membrane formation. *J. Cell Biol.* **213**, 479-494.
Fidler, A. L., Darris, C. E., Chetyrkin, S. V., Pedchenko, V. K., Boudko, S. P., Brown, K. L., Gray Jerome, W., Hudson, J. K., Rokas, A. and Hudson, B. G. (2017). Collagen IV and basement membrane at the evolutionary dawn of metazoan tissues. *eLife* **6**, e15040.
Fidler, A. L., Vanacore, R. M., Chetyrkin, S. V., Pedchenko, V. K., Bhave, G., Yin, V. P., Stothers, C. L., Rose, K. L., Mcdonald, W. H., Clark, T. A. et al. (2014). A unique covalent bond in basement membrane is a primordial innovation for tissue evolution. *Proc. Natl. Acad. Sci. USA* **111**, 331-336.
Flood-Page, P., Menzies-Gow, A., Phipps, S., Ying, S., Wangoo, A., Ludwig, M. S., Barnes, N., Robinson, D. and Kay, A. B. (2003). Anti-IL-5 treatment reduces deposition of ECM proteins in the bronchial subepithelial basement membrane of mild atopic asthmatics. *J. Clin. Invest.* **112**, 1029-1036.
Fox, J. W. Mayer, U., Nischt, R., Aumailley, M., Reinhardt, D., Wiedemann, H., Mann, K., Timpl, R., Krieg, T. and Engel, J. (1991). Recombinant nidogen consists of three globular domains and mediates binding of laminin to collagen type IV. *EMBO J.* **10**, 3137-3146.
Gustafsson, M. G. L., Shao, L., Carlton, P. M., Wang, C. J. R., Golubovskaya, I. N., Cande, W. Z., Agard, D. A. and Sedat, J. W. (2008). Three-dimensional resolution doubling in wide-field fluorescence microscopy by structured illumination. *Biophys. J.* **94**, 4957-4970.
Hopf, M., Göhring, W., Kohfeldt, E., Yamada, Y. and Timpl, R. (1999). Recombinant domain IV of perlecan binds to nidogens, laminin-nidogen complex, fibronectin, fibulin-2 and heparin. *Eur. J. Biochem.* **259**, 917-926.
Huber, A. R. and Weiss, S. J. (1989). Disruption of the subendothelial basement membrane during neutrophil diapedesis in an in vitro construct of a blood vessel wall. *J. Clin. Invest.* **83**, 1122-1136.
Karpowicz, P., Perez, J. and Perrimon, N. (2010). The Hippo tumor suppressor pathway regulates intestinal stem cell regeneration. *Development* **137**, 4135-4145.
Kleinman, H. K. and Martin, G. R. (2005). Matrigel: basement membrane matrix with biological activity. *Semin. Cancer Biol.* **15**, 378-386.
Kleinman, H. K., Mcgarvey, M. L., Liotta, L. A., Robey, P. G., Tryggvason, K. and Martin, G. R. (1982). Isolation and characterization of type IV procollagen, laminin, and heparan sulfate proteoglycan from the EHS sarcoma. *Biochemistry* **21**, 6188-6193.
Kleinman, H. K., Mcgarvey, M. L., Hassell, J. R., Star, V. L., Cannon, F. B., Laurie, G. W. and Martin, G. R. (1986). Basement membrane complexes with biological activity. *Biochemistry* **25**, 312-318.
Langeveld, J. P., Noelken, M. E., Hård, K., Todd, P., Vliegenthart, J. F., Rouse, J. and Hudson, B. G. (1991). Bovine glomerular basement membrane. Location and structure of the asparagine-linked oligosaccharide units and their potential role in the assembly of the 7 S collagen IV tetramer. *J. Biol. Chem.* **266**, 2622-2631.
Li, H., Qi, Y. and Jasper, H. (2013). Dpp signaling determines regional stem cell identity in the regenerating adult drosophila gastrointestinal tract. *Cell Rep.* **4**, 10-18.
Li, S., Qi, Y., Mckee, K., Liu, J., Hsu, J. and Yurchenco, P. D. (2017). Integrin and dystroglycan compensate each other to mediate laminin-dependent basement membrane assembly and epiblast polarization. *Matrix Biol.* **57-58**, 272-284.
Maartens, A. P. and Brown, N. H. (2015). The many faces of cell adhesion during Drosophila muscle development. *Dev. Biol.* **401**, 62-74.
Mccall, A. S., Cummings, C. F., Bhave, G., Vanacore, R., Page-Mccaw, A. and Hudson, B. G. (2014). Bromine is an essential trace element for assembly of

collagen IV scaffolds in tissue development and architecture. *Cell* **157**, 1380-1392.
Mercuri, E. and Muntoni, F. (2013). Muscular dystrophies. *The Lancet* **381**, 845-860.
Nyström, A., Bornert, O. and Kühl, T. (2017). Cell therapy for basement membrane-linked diseases. *Matrix Biol.* **57-58**, 124-139.
Page-McCaw, A. Serano, J., Santé, J. M. and Rubin, G. M. (2003). Drosophila matrix metalloproteinases are required for tissue remodeling, but not embryonic development. *Dev. Cell* **4**, 95-106.
Pastor-Pareja, J. C. and Xu, T., (2011). Shaping cells and organs in Drosophila by opposing roles of fat body-secreted Collagen IV and perlecan. *Dev. Cell* **21**, 245-256.
Poritz, L. S., Garver, K. I., Green, C., Fitzpatrick, L., Ruggiero, F. and Koltun, W. A. (2007). Loss of the tight junction protein ZO-1 in dextran sulfate sodium induced colitis. *J. Surg. Res.* **140**, 12-19.
Pöschl, E., Schlötzer-Schrehardt, U., Brachvogel, B., Saito, K., Ninomiya, Y. and Mayer, U. (2004). Collagen IV is essential for basement membrane stability but dispensable for initiation of its assembly during early development. *Development* **131**, 1619-1628.
Ramos-Lewis, W. and Page-McCaw, A. (2018). Basement membrane mechanics shape development: lessons from the fly. *Matrix Biol.* **75**, 72-81.
Ramos-Lewis, W., Lafever, K. S. and Page-McCaw, A. (2018). A scar-like lesion is apparent in basement membrane after wound repair in vivo. *Matrix Biol.* **75**, 101-120.
Ren, F., Wang, B., Yue, T., Yun, E.-Y., Ip, Y. T. and Jiang, J. (2010). Hippo signaling regulates Drosophila intestine stem cell proliferation through multiple pathways. *Proc. Natl. Acad. Sci. USA* **107**, 21064-21069.
Ren, F. Shi, Q., Chen, Y., Jiang, A., Ip, Y. T., Jiang, H. and Jiang, J. (2013). Drosophila Myc integrates multiple signaling pathways to regulate intestinal stem cell proliferation during midgut regeneration. *Cell Res.* **23**, 1133-1146.
Rera, M. Bahadorani, S., Cho, J., Jiang, A., Koehler, C. L., Ulgherait, M., Hur, J. H.Ansari, W. S. Lo, T., Jones, D. L. and Walker, D. W. (2011). Modulation of longevity and tissue homeostasis by the Drosophila PGC-1 homolog. *Cell Metab.* **14**, 623-634.
Ries, A., Göhring, W., Fox, J. W., Timpl, R. and Sasaki, T. (2001). Recombinant domains of mouse nidogen-1 and their binding to basement membrane proteins and monoclonal antibodies. *Eur. J. Biochem.* **268**, 5119-5128.
Risteli, J., Timpl, R., Bachinger, H. P., Engel, J. and Furthmayr, H. (1980). 7-S collagen: characterization of an unusual basement membrane structure. *Eur. J. Biochem.* **108**, 239-250.
Shimamoto, Y. and Kapoor, T. M. (2012). Microneedle-based analysis of the micromechanics of the metaphase spindle assembled in Xenopus laevis egg extracts. *Nat. Protoc.* **7**, 959-969.
Soudi, M., Zamocky, M., Jakopitsch, C., Furtmüller, P. G. and Obinger, C. (2012). Molecular evolution, structure, and function of peroxidasins. *Chem. Biodivers.* **9**, 1776-1793.
Sugimoto, H., Mundel, T. M., Sund, M., Xie, L., Cosgrove, D. and Kalluri, R. (2006). Bone-marrow-derived stem cells repair basement membrane collagen defects and reverse genetic kidney disease. *Proc. Natl. Acad. Sci. USA* **103**, 7321-7326.
Suleiman, H., Zhang, L., Roth, R., Heuser, J. E., Miner, J. H., Shaw, A. S. and Dani, A. et al. (2013). Nanoscale protein architecture of the kidney glomerular basement membrane. *eLife* **2**, 1471.
Takagi, J., Yang, Y., Liu, J.-, Wang, J.- and Springer, T. A. (2003). Complex between nidogen and laminin fragments reveals a paradigmatic beta-propeller interface. *Nature* **424**, 969-974.
Tian, A. and Jiang, J. (2014). Intestinal epithelium-derived BMP controls stem cell self-renewal in Drosophila adult midgut. *eLife* **3**, e01857.
Tian, A., Shi, Q., Jiang, A., Li, S., Wang, B. and Jiang, J. (2015). Injury-stimulated Hedgehog signaling promotes regenerative proliferation of Drosophila intestinal stem cells. *J. Cell Biol.* **208**, 807-819.
Tsilibary, E. C. (2003). Microvascular basement membranes in diabetes mellitus. *J. Pathol.* 200, 537-546.
Urbano, J. M., Torgler, C. N., Molnar, C., Tepass, U., Lopez-Varea, A., Brown, N. H., De Celis, J. F. and Martin-Bermudo, M. D. (2009). Drosophila laminins act as key regulators of basement membrane assembly and morphogenesis. *Development* **136**, 4165-4176.
Vanacore, R. Ham, A.-J. L., Voehler, M., Sanders, C. R., Conrads, T. P., Veenstra, T. D., Sharpless, K. B., Dawson, P. E. and Hudson, B. G. (2009). A sulfilimine bond identified in collagen IV. *Science* **325**, 1230-1234.
Vila, M. C. Rayavarapu, S., Hogarth, M. W., Van Der Meulen, J. H., Horn, A., Defour, A., Takeda, S., Brown, K. J., Hathout, Y., Nagaraju, K. et al. (2017). Mitochondria mediate cell membrane repair and contribute to Duchenne muscular dystrophy. *Cell Death Differ.* **24**, 330-342.
Wang, X., Harris, R. E., Bayston, L. J. and Ashe, H. L. (2008). Type IV collagens regulate BMP signalling in Drosophila. *Nature* **455**, 72-77.
Wolfstetter, G., Dahlitz, I., Pfeifer, K., Töpfer, U., Alt, J. A., Pfeifer, D. C., Lakes-Harlan, R., Baumgartner, S., Palmer, R. H. and Holz, A. (2019). Characterization of Drosophila Nidogen/entactin reveals roles in basement membrane stability, barrier function and nervous system patterning. *Development* **146**, dev168948.
Xiao, Y. S., Schöck, F. and González-Morales, N. (2017). Rapid IFM dissection for visualizing fluorescently tagged sarcomeric proteins. *Bio Protoc.* **7**, e2606.
You, J., Zhang, Y., Li, Z., Lou, Z., Jin, L. and Lin, X. (2014). Drosophila perlecan regulates intestinal stem cell activity via cell-matrix attachment. *Stem Cell Reports* **2**, 761-769.
Yurchenco, P. D. (2011). Basement membranes: cell scaffoldings and signaling platforms. *Cold Spring Harbor Perspect. Biol.* **3**, a004911-a004911.
Yurchenco, P. D. and Furthmayr, H. (1984). Self-assembly of basement membrane collagen. *Biochemistry* **23**, 1839-1850.
Yurchenco, P. D., Tsilibary, E. C., Charonis, A. S. and Furthmayr, H. (1985). Laminin polymerization in vitro. Evidence for a two-step assembly with domain specificity. *J. Biol. Chem.* **260**, 7636-7644.
Yurchenco, P. D., Cheng, Y. S. and Colognato, H. (1992). Laminin forms an independent network in basement membranes. *J. Cell Biol.* **117**, 1119-1133.

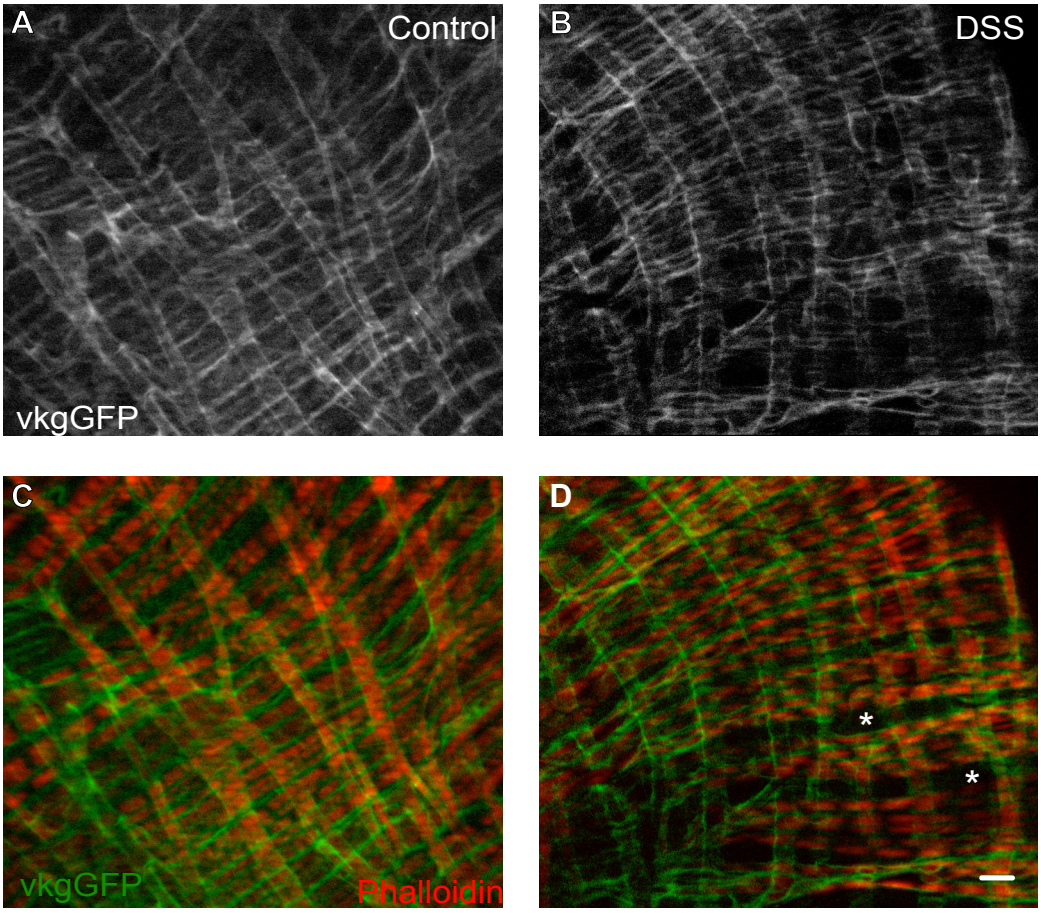

Fig. S1. Surface view of the gut basement membrane after DSS feeding.

(A) Tangential view of the gut basement membrane (Vkg-GFP) in control-fed flies. **(B)** Tangential view of gut basement membrane in DSS-fed flies. **(C-D)** Merged images of above showing the basement membrane (green) surrounding the muscles (phalloidin, red). Apparent "holes" in basement membrane (asterisks in D) represent areas where the muscles have separated. Scale bar= 10 μm.

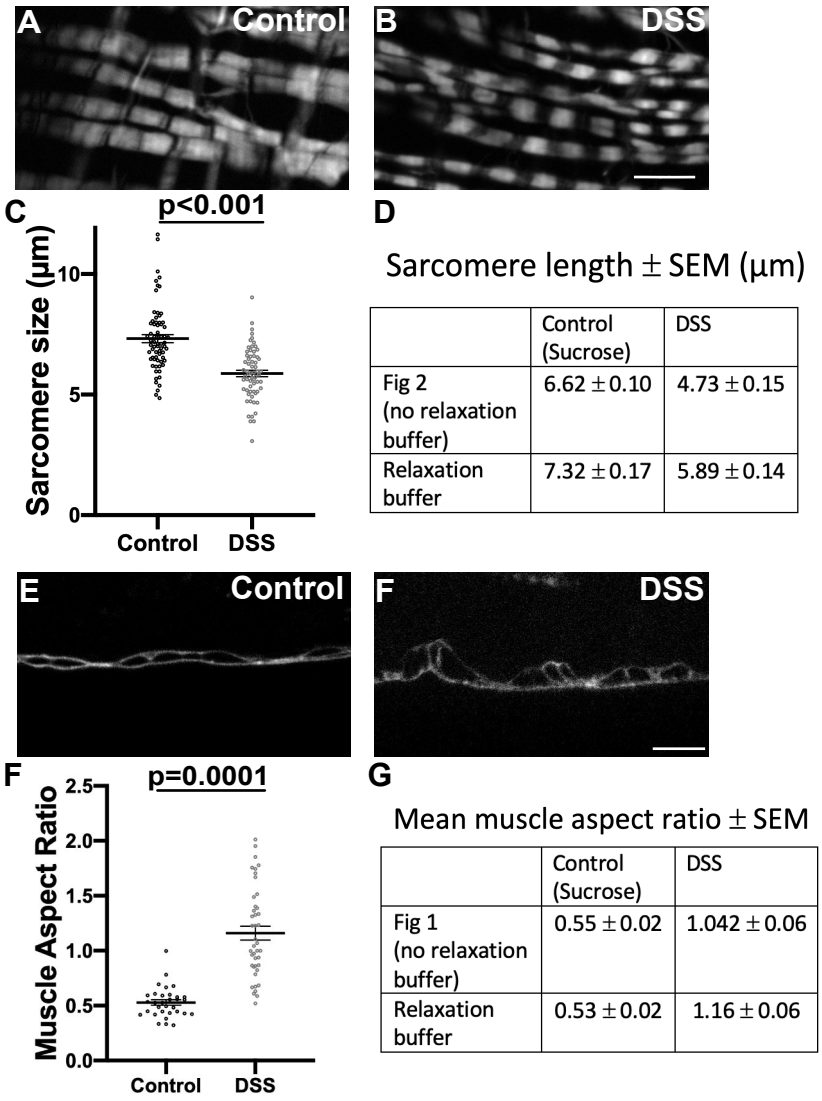

	Control (Sucrose)	DSS
Fig 2 (no relaxation buffer)	6.62 ± 0.10	4.73 ± 0.15
Relaxation buffer	7.32 ± 0.17	5.89 ± 0.14

	Control (Sucrose)	DSS
Fig 1 (no relaxation buffer)	0.55 ± 0.02	1.042 ± 0.06
Relaxation buffer	0.53 ± 0.02	1.16 ± 0.06

Fig. S2. DSS muscle damage is still evident when guts are treated with relaxing buffer.

Midguts from DSS-fed and control flies were dissected and incubated in relaxing buffer to allow muscle relaxation before analysis.

(A-B) Phalloidin staining to show sarcomeres in midgut longitudinal muscles dissected in relaxing buffer. **(C)** Sarcomere length is still significantly shorter in DSS fed flies than control-fed flies, indicating that muscles are damaged and not simply contracted by DSS. **(D)** Relaxing buffer did cause moderate lengthening of sarcomeres in both control and DSS fed flies when compared to sarcomere sizes from Fig. 2.

(E-F) Vkg-GFP outlines were used to calculate the cirumferential muscle aspect ratio of guts treated with relaxing buffer. (**G)** Muscle aspect ratio is still significantly greater in DSS fed flies than control fed flies, indicating that muscles are damaged and not simply contracted by DSS. (**H)** Relaxation buffer had little effect on the aspect ratio

Scale bars = 10 µm

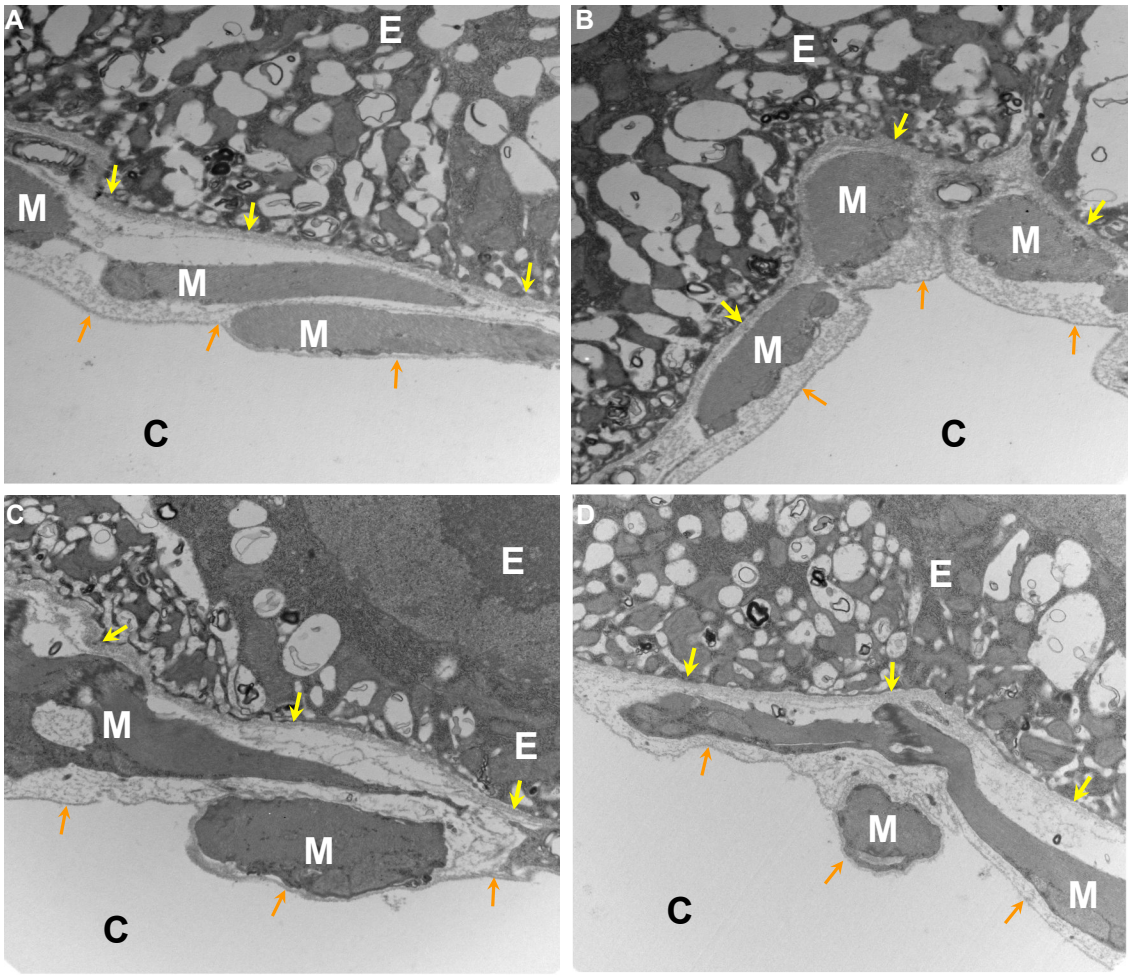

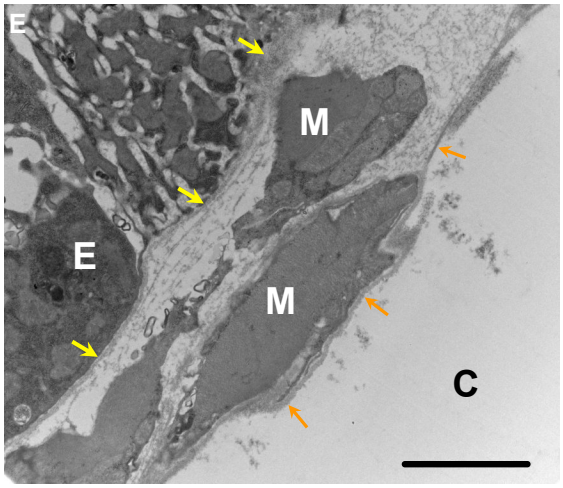

E- enterocyte epithelial layer.

C- body cavity.

M - muscle.

Scale bar = 2 μm

Fig. S3. The basement membranes of control midguts show a variety of morphologies.

A-E. TEM images of control wild-type (w^{1118}) midguts, fed 48 h on a sucrose diet. The longitudinal and circumferential muscles are perpendicularly oriented to each other. In TEM images, the longitudinal muscles appear round in cross-section, whereas circumferential muscles appear long, because guts were cut in cross-section. In contrast, SIM and optical sections are taken along the long axis, so that the circumferential mucles appear round and longitudinal muscles appear long as shown in Fig. 1A. Either circumferential or longitudinal muscles can be found next to the body cavity (see also Figs. 3A and 5B), leading us to conclude that the longitudinal and circumferential muscles are in some kind of basket weave pattern, as depicted in Fig. 1A.

Sheet-like basement membranes are observed 1) underneath the epithelial enterocyte layer, indicated by yellow arrows, and 2) outside the muscles separating them from the body cavity, indicated by orange arrows. The structure of the material between these two layers is unclear, although SIM imaging indicates that the material between and around the muscles contains collagen IV even though it is not organized into a sheet (Figs. 3D and 7A).

Journal of Cell Science • Supplementary information

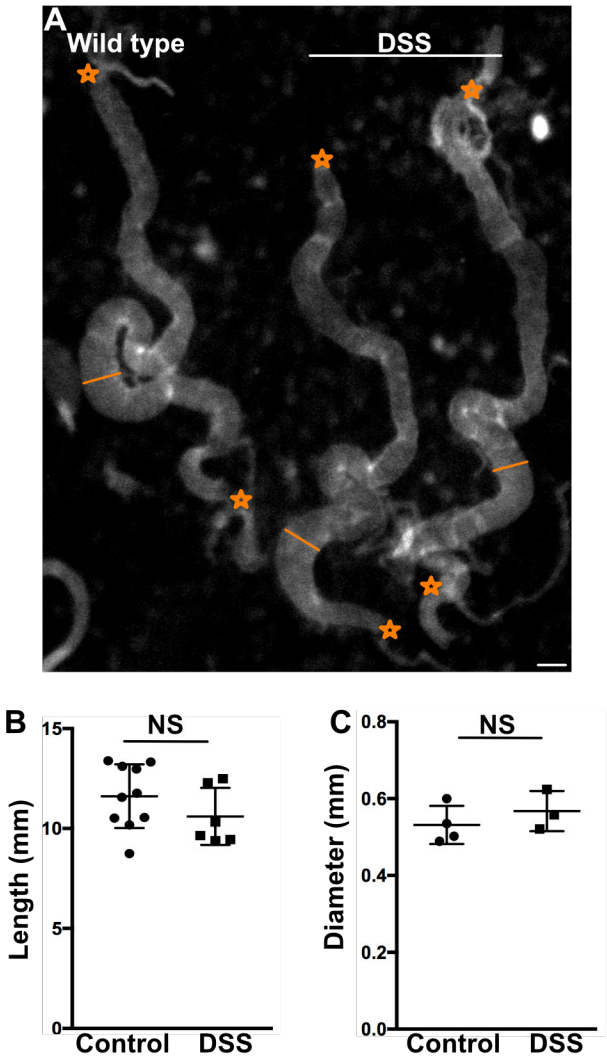

Fig. S4. DSS has no significant effect on the length or diameter of the gut.

(A) Brightfield image of guts dissected from control flies. The entire gut length is measured as the distance between the two stars, top and bottom. The diameter is measured as indicated by the orange line across the midgut. **(B-C)** Neither the length (B) or diameter (C) was significantly changed between animals fed DSS vs control food for 48 h. Scale bar = 500 μm

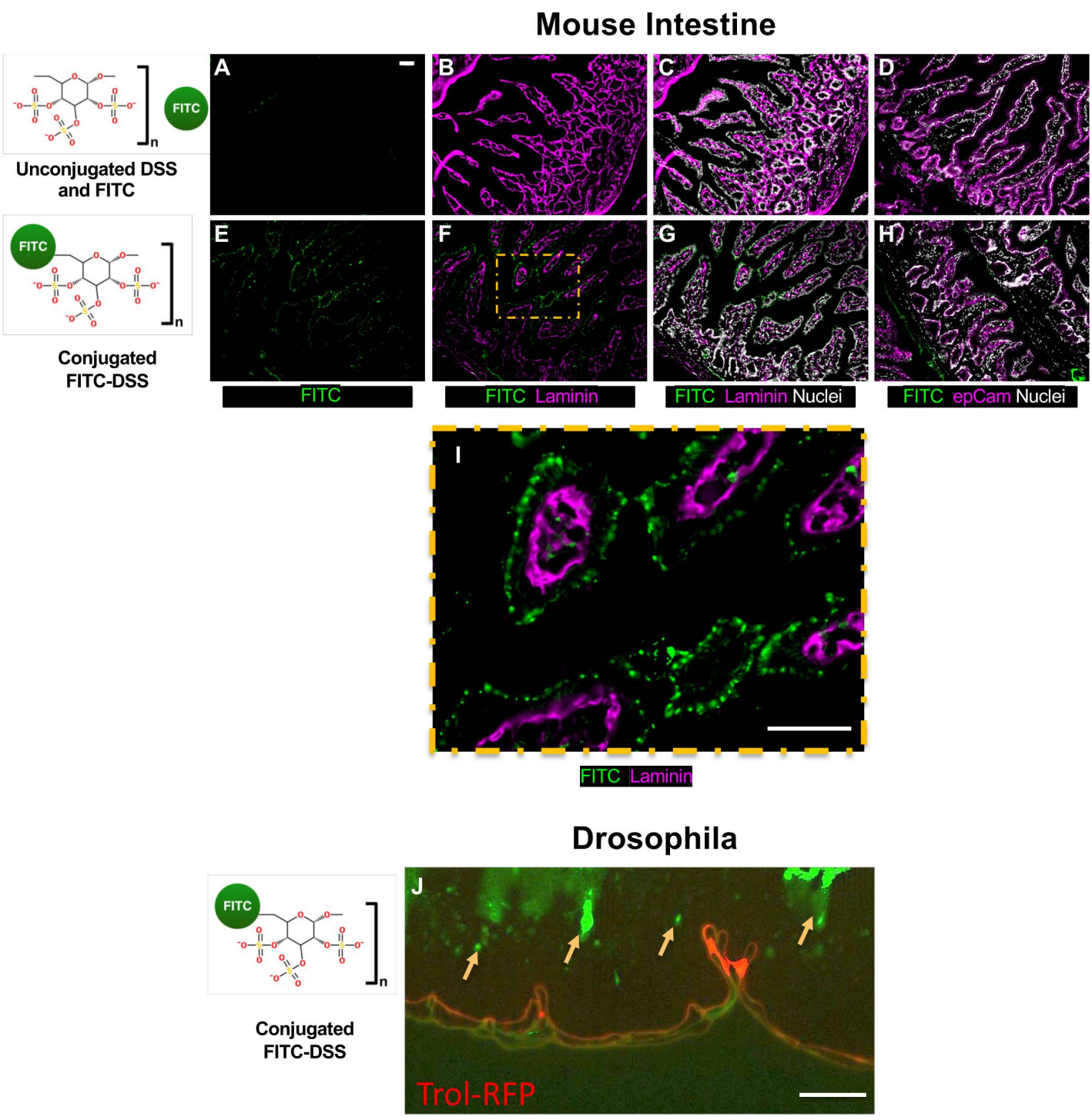

Fig. S5. In mice, DSS does not accumulate in intestinal basement membranes but rather at cellular junctions.

(A-D) Intestines from control mice administered DSS and unconjugated FITC. (A-C) represent the same sample stained for the basement membrane protein laminin, whereas (D) was stained for E-cadherin. No clear FITC signal is observed (A).

(E-H) Intestines from mice administered FITC-DSS. (E-G) represent the same sample stained for the basement membrane protein laminin, whereas (H) was stained for E-cadherin. FITC-DSS localized in punctae (E) that did not colocalize with laminin. Rather, FITC-DSS localized near the epithelial plasma membrane, stained with E-Cadherin (H). **(I)** A magnified region of F showing FITC-DSS does not co-localize with the basement membrane. Scale bar= 50 μm.

(J) Drosophila guts with FITC-DSS evident in the enterocytes, likely during transport. The lumen is omitted from the top of the image because it is significantly brighter. Scale bar = 10 μm.

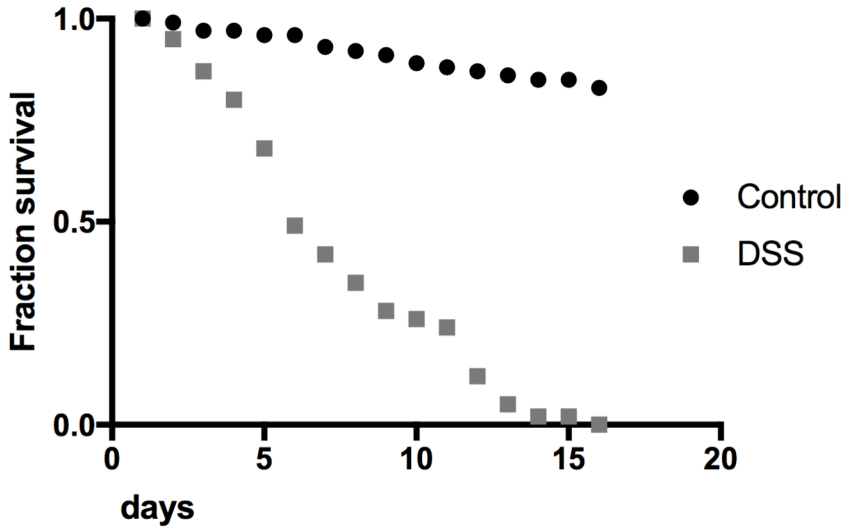

Fig. S6. Flies fed DSS have an increased mortality rate.

Flies continuously fed DSS for 16 days die rapidly compared to controls. These results are similar to those reported by Amcheslavsky et al (2009).

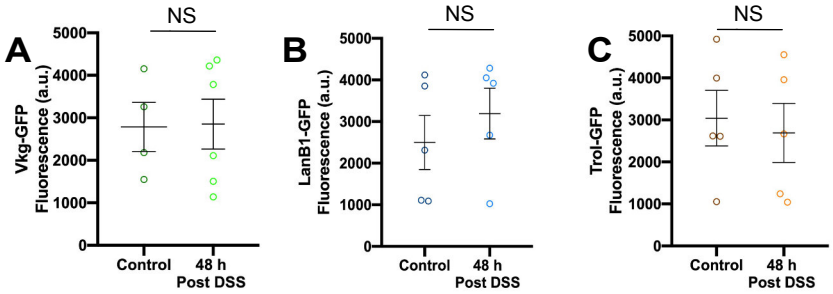

Fig. S7. Basement membrane protein levels were not significantly different after repair.

(A-C) Basement membrane protein levels were not significantly different in control vs. DSS-fed midguts allowed to recover for 48 h, as indicated by fluorescence levels of Vkg-GFP (A), LanB1-GFP (B) or Trol-GFP (C). Fluorescence was measured 48 h after removal from DSS to normal food; controls were sucrose-fed for 48 h then switched to normal food for 48 h to match experimental conditions. Each dot represents one gut.

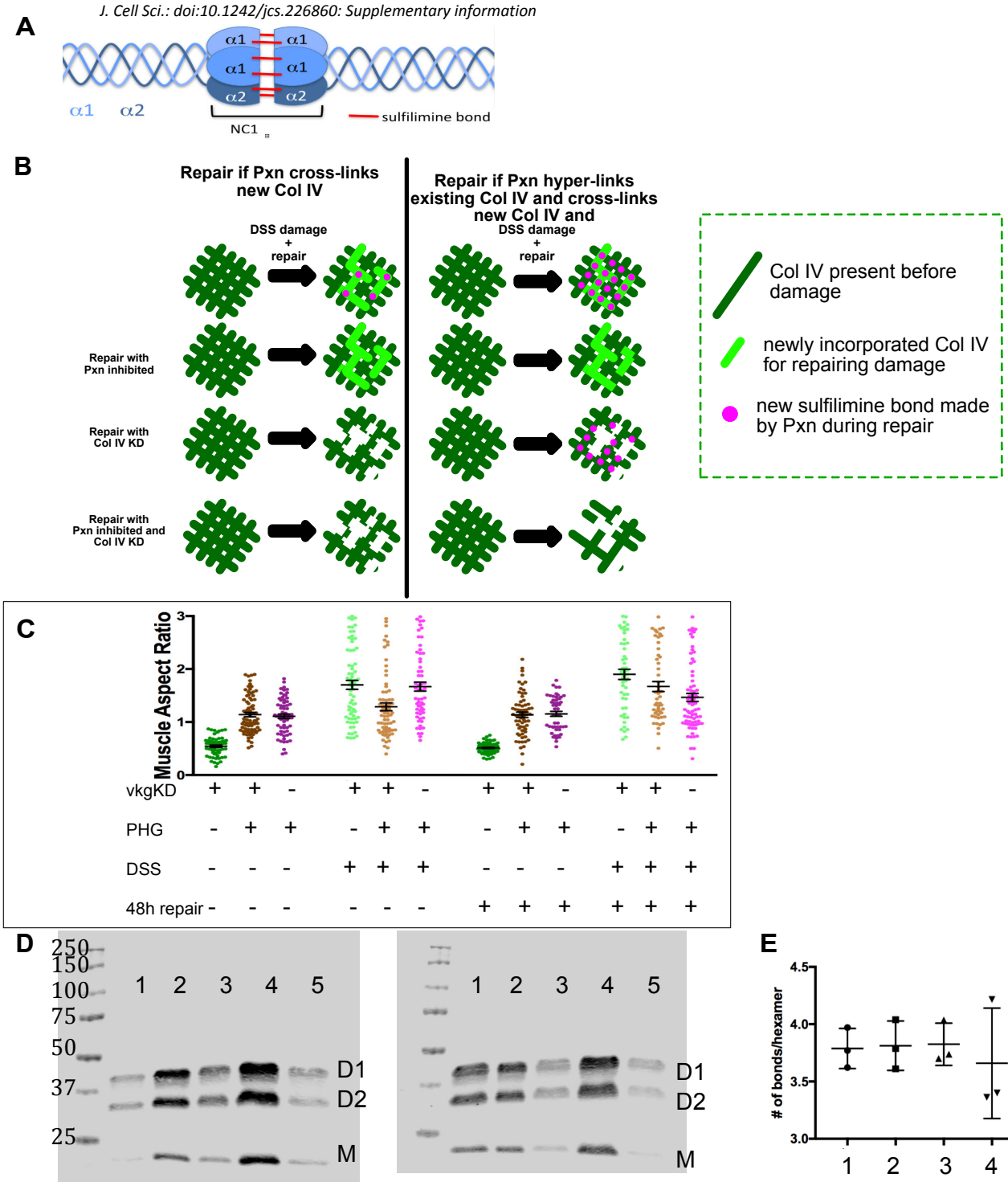

Fig. S8. Peroxidasin does not hypercrosslink basement membrane during repair.

(A) Schematic showing 6 possible sulfilimine bonds per NC1 hexamer. **(B)** Models illustrate how loss of both collagen IV and Pxn are expected to affect repairing basement membrane: (left) Pxn is required only to crosslink the newly inserted collagen IV; (right) Pxn hypercrosslinks the basement membrane to stabilize it as part of the repair process. **(C)** Muscle aspect ratios after *vkg* knockdown (with *TubP-Gal4, Gal80ts*), Pxn inhbition by PHG, or both treatments, after control or DSS feeding, with or without a repair period of 48h after DSS withdrawal. Because the double treatment is not worse than the single treatments, we conclude that Pxn does not hypercrosslink collagen IV during repair. **(D)** 2 western blots of gut samples showing the Collagen IV NC1 domain, which has altered electrophoretic mobility depending on its crosslinked status: D1 is a dimer with one sulfilimine crosslink, D2 is dimer with two sulfilimine crosslinks, and M is monomer without crosslinks. Lanes: 1-normal food, 2-sucrose, 3-DSS no recovery, 4-DSS 48 h recovery, and 5-PHG. **(E)** The number of sulfilimine bonds calculated per hexamer of the 5 different condition types in 3 biological replicates. Sulfilimine crosslinking does not increase either after DSS treatment or repair.

Table S1. Statistics on Figure 7G*

Samples compared	P value†
Sibling Control	
A-B (0 h v 48 h, sucrose)	ns
A-C (0 h sucrose v 0 h DSS)	<0.001
B-D (48 h sucrose v 48 h DSS)	ns
C-D (0 h v 48 h, DSS)	<0.001
Pxn-KD	
E-F (0 h v 48 h, sucrose)	0.007
E-G (0 h sucrose v 0 h DSS)	<0.001
F-H (48 h sucrose v 48 h DSS)	<0.001
G-H (0 h v 48 h, DSS)	ns

* Columns in Figure 7G are lettered alphabetically left to right
† ANOVA with unpaired t-tests with a Bonferroni correction

Table S2. Statistics on Figure 7N*

Samples compared	P value†
Sibling Control	
A-B (0 h v 48 h, sucrose)	ns
A-C (0 h sucrose v 0 h DSS)	<0.001
B-D (48 h sucrose v 48 h DSS)	ns
C-D (0 h v 48 h, DSS)	<0.001
Pxn-KD	
E-F (0 h v 48 h, sucrose)	ns
E-G (0 h sucrose v 0 h DSS)	<0.001
F-H (48 h sucrose v 48 h DSS)	<0.001
G-H (0 h v 48 h, DSS)	ns
PHG	
I-J (0 h v 48 h, sucrose)	0.04
I-K (0 h sucrose v 0 h DSS)	<0.001
J-L (48 h sucrose v 48 h DSS)	<0.001
K-L (0 h v 48 h, DSS)	<0.001

* Columns in Figure 7N are lettered alphabetically left to right
† ANOVA with unpaired t-tests with a Bonferroni correction

Table S3. Statistics on Figure 8J*

Samples compared	P value†
Sibling Control	
A-B (0 h v 48 h, sucrose)	ns
A-C (0 h sucrose v 0 h DSS)	<0.001
B-D (48 h sucrose v 48 h DSS)	ns
C-D (0 h v 48 h DSS)	<0.001
Vkg-KD	
E-F (0 h v 48 h, sucrose)	ns
E-G (0 h sucrose v 0 h DSS)	<0.001
F-H (48 h sucrose v 48 h DSS)	<0.001
G-H (0 h v 48 h, DSS)	0.001
LanB1-KD	
I-J (0 h v 48 h, sucrose)	ns
I-K (0 h sucrose v 0 h DSS)	<0.001
J-L (48 h sucrose v 48 h DSS)	<0.001
K-L (0 h v 48 h, DSS)	ns

* Columns in Figure 8J are lettered alphabetically left to right
† ANOVA with unpaired t-tests with a Bonferroni correction

Table S4. Drosophila lines used in this study.

Genotype	Source	Used for
w^{1118}	Todd Laverty, Janelia Farm	Figs. 2, 3, 4, 5, 6, S2, S3, S4, S6
w; vkg-GFP^{454}	Yale Flytrap Project	Figs. 1, 3, 7, 8, S1, S2, S7, S8
w; LanB1-GFP	VDRC 318180	Figs. 1, 3, S7
trol-GFP^{1700} *w*	Flytrap line ZCL1973	Figs. 1, 3, S7
y trol-RFP w	Vincent Mirouse, French National Centre for Scientific Research	Figs. 4, S5
w; UAS-vkg^{RNAi}	VDRC 106812	Figs. 8, S8
w; UAS-vkg^{RNAi}	VDRC 41278	Not shown
w; *UAS-LanB1*^{RNAi}	VDRC 23121	Figs. 2, 8
w; *UAS-LanB1*^{RNAi}	VDRC 23119	Not shown
w; vkg-GFP^{454}*/CyO; UAS-Pxn*^{RNAi} */ TubP-Gal4, TubP-Gal80*^{ts}	This study; VDRC 15276	Figs. 1, 7
w UAS- Pxn^{RNAi}/FM7c	VDRC 15277	Not shown
w; *vkg-GFP*^{205}; *TubP-Gal4*, *TubP-Gal80*^{ts}*/SM6-TM6B*	Ramos-Lewis et. al. 2018	Fig. 8
w; *LanB1-GFP TubGal4 TubP-Gal80*^{ts}*/TM6B*	Ramos-Lewis et. al. 2018	Figs. 8, S8